Title: Morphofunctional deficits in the cerebral cortex of NeuroD2 mutant mice are associated with autism/schizophrenia-like behaviors

Running title: Autism/Schizophrenia-like phenotypes in NeuroD2 KO mice

*Stéphane Bugeon [1] *, Sahra Lafi [1,2] *, Corinne Beurrier [1 &], Surajit Sahu [2 &], Karen Runge [2], Fabienne Schaller [2], Arthur Loubat [2], Rémi Mathieu [2], Leonard Herault [3], Stéphane Gaillard [4], Mélanie Cahuc [2], Emilie Pallesi-Pocachard [2], Aurélie Montheil [2], Andreas Bosio [5], Alfonso Represa [2], Carlos Cardoso [2], Harold Cremer [1] and Antoine de Chevigny [1,2,6]*

[1] IBDM, Aix-Marseille University, CNRS, UMR 7288, Marseille, France

[2] INMED INSERM U901, Aix-Marseille University, Marseille, France

[3] TAGC INSERM U1090, Aix-Marseille University, Marseille, France

[4] Phenotype Expertise, 5 Boulevard du Maréchal Koenig, 13009 Marseille, France

[5] Miltenyi Biotec, Bergisch-Gladbach 51429, Germany.

[6] Author for correspondence:

Antoine de Chevigny, PhD

Research Associate

INMED INSERM U901

Campus de Luminy

13273 Marseille Cédex 09

antoine.de-chevigny@inserm.fr

+33 4 91 82 81 84

*, & equal contribution

The Authors declare no competing interests

Abstract:

The transcription factor NeuroD2 is a recent candidate for neuropsychiatric disorders but its impact in cortical networks and associated behaviors remains unknown. Here we show that in the mouse neocortex, NeuroD2 is restricted to pyramidal neurons, from development to adulthood. In NeuroD2 deficient mice, layer 5 pyramidal neurons of motor area displayed reduced dendritic complexity and reduced spine density. In contrast, production, radial migration, laminar organization and axonal target specificity of pyramidal neurons were normal, revealing a synaptopathy phenotype. Electrophysiologically, intrinsic excitability and inhibitory inputs onto pyramidal neurons were increased. Behaviorally, NeuroD2 homozygous and heterozygous mice exhibited normal interest and memory for objects but altered sociability and social memory, stereotypies, spontaneous epilepsy and hyperactivity. RNA sequencing from microdissected neocortex revealed that NeuroD2 target genes are highly associated with in cell intrinsic excitability, synaptic regulation, autism and schizophrenia. These results strongly reinforce the potential implication of NeuroD2 mutations in human neuropsychiatric disorders.

Keywords: cortical pyramidal neurons, NeuroD2 transcription factor, intrinsic excitability, dendrites and spines, autism/schizophrenia

Introduction

Alterations in synaptic transmission, neuronal excitability and/or of excitation/inhibition balance in pyramidal neurons (PNs) of the neocortex are emerging theories of the pathophysiology of several neurodevelopmental and neuropsychiatric disorders including autism spectrum disorders (ASD) and schizophrenia (SCZ) (Rubenstein and Merzenich, 2003; Zoghbi and Bear, 2012). Despite a field of intense investigation, the factors that regulate synaptic transmission or cell intrinsic excitability in cortical PNs remain poorly understood.

NeuroD2 belongs to the family of NeuroD basic helix-loop-helix transcription factor that bind genomic E boxes (CANNTG) to regulate neuronal differentiation during development (Lee *et al.*, 1995). While cortical expression of its closest and first identified paralog NeuroD1 is turned off around birth (Lee *et al.*, 1995), NeuroD2 cortical expression persists postnatally (McCormick *et al.*, 1996), suggesting that it might be involved in processes other than early neuronal differentiation (Lee *et al.*, 1995). Interestingly, NeuroD2-mediated transcription is regulated by neuronal activity in cultured cortical PNs (Ince-Dunn *et al.*, 2006). Moreover, few studies indicate that NeuroD2 might regulate synaptic formation and/ or function in the hippocampus (Wilke *et al.*, 2012), amygdala (Lin *et al.*, 2005) and cerebellum (Yang *et al.*, 2009). Finally, rare single nucleotide polymorphisms in NeuroD2 are associated with risks of schizophrenia (Spellmann *et al.*, 2017). Together, the current evidence suggests that NeuroD2 might be involved in synaptic formation in the cerebral cortex and thus be related with neurodevelopmental and neuropsychiatric disorders.

Here, we analyze the development of the cerebral cortex in NeuroD2 constitutive knockout (KO) mice, by focusing on layer 5 of the motor area because it has been associated with ASD (Willsey *et al.*, 2013) and SCZ (Benes *et al.*, 1986) in humans. We find that NeuroD2 KO PNs display molecular, anatomical and electrophysiological alterations, which correlate with behaviors that are highly relevant to neurodevelopmental and neuropsychiatric disorders such as ASD and SCZ. Indeed, while NeuroD2 deficiency does not alter migration, subtype specification, layer position and axonal targeting identity of PNs, it specifically reduces spine

density, increases cell intrinsic excitability and alters the expression of ASD and SCZ-associated genes as revealed by RNA deep sequencing. Behaviorally, NeuroD2 deficiency decreases sociability and social memory and induces ASD-comorbidity like behaviors such as epilepsy and hyperactivity. These extensive analyses support the potential implication of NeuroD2 mutations in human neuropsychiatric disorders.

Material & Methods:

Animals. Mice (mus musculus) were group housed (2–5 mice/cage; unless specified) with same-sex littermates on a 12 hr light-dark cycle with access to food and water ad libitum. NeuroD2 deficient mice were previously described (Bormuth *et al.*, 2013). Mice were bred and maintained on a mixed SVeV-129/C57BL/6J background. Experimenters were blinded to the mouse genotype during data acquisition and analysis. Animal experiments were carried out in accordance with European Communities Council Directive and approved by French ethical committees (Comité d'Ethique pour l'expérimentation animale no. 14; permission number: 62-12112012).

Histology - Immunohistochemistry.

Mice were perfused transcardially with ice-cold 4% paraformaldehyde (in PBS). Brains were removed and post-fixed overnight at 4°C with the same fixative. Coronal sections were cut at 50 um thickness using a cryostat (Leica) or a microtome (Microm).

Immunofluorescence experiments were performed as described before (de Chevigny *et al.*, 2012). Briefly, free-floating sections were blocked and permeabilized for one hour in a "blocking solution" composed of 10% Normal Goat Serum, 0.2% Triton X-100 (Sigma) in PBS. Primary antibodies, diluted in blocking solution and added overnight at 4°C, were as follows: rabbit anti-NeuroD2 (Abcam # 104430, 1:1000), rabbit anti-Tbr1 (Abcam, 1:1000), rat anti-Ctip2 (Abcam # ab18465, 1:100), mouse anti-Satb2 (Abcam # ab51502, 1:500). Corresponding fluorescently labeled secondary antibodies (AlexaFluor, Invitrogen) were added for 2 hours in blocking solution. Hoechst was added in PBS for 10 minutes, and sections were mounted on microscope slides that were coversliped using Mowiol solution (Sigma).

Quantitative reverse transcription polymerase chain reaction (qRT-PCR). Total RNAs were extracted from whole cortex (for developmental expression of NeuroD2, Fig. S1) taken at various developmental stages (E14.5, E16.5, E18.5, P7, P14 and P30) (n = 3-4 brains per

stage in each condition), or from motor plus somatosensory areas (Fig. 5a, n=3 samples per condition) using TRIZOL reagent according to manufacturer's instructions (Life Technology). cDNA was synthesized from 1 µg of total RNA using Quantitect Reverse Transcription Kit and according to manufacturer protocol (Qiagen). RT-PCRs were then carried out using SYBR-Green chemistry (Roche Diagnostics) and Roche amplification technology (Light Cycler 480). PCR primers (Table below) were designed for 12 mouse genes, and for 3 control genes, cyclo-oxigenase 2 (COX2), Ribosomal protein L13a (Rpl13a) and HPRT for relative quantification. All primer pairs were optimized to ensure specific amplification of the PCR product and the absence of any primer dimer. Quantitative PCR standard curves were set up for all. Values of fold change represent averages from duplicate measurements for each sample.

Gene	Forward	Reverse
NeuroD2	AAGCCAGTGTCTCTTCGTGG	GCCTTGGTCATCTTGCGTTT
Scn4b	GAACCGAGGCAATACTCAGG	ACGACAGGTACATGGGAAGC
Kcnk4	CACTCACTGGCCTGGACAA	GAGCTCCTGGGGAGCAGT
Scn8a	CAAGCTGGAGAATGGAGGCA	TAAGAGGGGAGGGAGGCTGT
Kcnh1	GGTGAGAATGTTCACAAGCACT	ACTGGGGAAGGATGTCTGAA
Scn1a	GGTTTGAGACCTTCATTGTGTTC	TTTTGATCGTCTTTCGCTGA
Kcnq5	TACAGGAGCAGCACCGCCAG	CCTTGTTCTTTCTTGGTAGGGC
Cacna1c	CCCTTCTTGTGCTCTTCG TC	TTGTGCATCTTTCCCATG AA
Grin2b	TGCTGTAGCTGTCTTTGTCTTTG	CTTTGCCGATGGTGAAAGAT
Htr2a	CTGCTGGGTTTCCTTGTCAT	GTAAATCCAGACGGCACAGAG
Cdh8	GTGACCCTGATATCACTTCCAGT	TCTTCCCATCATCTGCATTG
Ppia1	QT00247709	QT00247709
Rpl13a	CCCTCCACCCTATGACAAGA	GCCCCAGGTAAGCAAACTT
HPRT	QT00166768	QT00166768

***In vitro* electrophysiology.** Coronal slices (250 µm) from 21 to 30 days-old mice were cut with a VT 1000S vibratome (Leica) in ice-cold high-choline artificial cerebro-spinal fluid (ACSF) containing (in mM): 130 choline, 2.5 KCl, 1.25 NaH_2PO_4, 7 $MgCl_2$, 0.5 $CaCl_2$, 25 $NaHCO_3$ and 7 glucose at 4°C. Slices were then maintained at room temperature in oxygenated ACSF containing (in mM): 126 NaCl, 2.5 KCl, 1.2 NaH_2PO_4, 1.2 $MgCl_2$, 2.4 $CaCl_2$, 25 $NaHCO_3$ and 11 glucose, to which 250 µM kynurenic acid and 1 mM sodium pyruvate were added. Slices were then transferred one at a time to a submersion recording chamber and were perfused continuously with ACSF warmed to 33°C at a rate of 2.5-3 ml/min. All solutions were equilibrated with 95% O_2/5% CO_2. Neurons were visualized on an

upright microscope (Nikon Eclipse FN1) equipped with DIC optic and filter set to visualize EYFP using a x40 water-immersion objective. Recordings were interleaved in control and NeuroD2 KO mice.

Miniature excitatory and inhibitory postsynaptic currents (mEPSCs and mIPSCs, respectively) were recorded in whole-cell configurations in voltage-clamp mode in oxygenated ACSF containing tetrodotoxin (TTX, 1 μM). Patch-clamp electrodes (4-6 MΩ) were filled with an intracellular solution of the following composition (in mM): 120 $CsMeSO_4$, 12.3 CsCl, 0.1 $CaCl_2$, 1 EGTA, 10 HEPES, 4 MgATP, 0.3 NaGTP, pH adjusted to 7.25 with CsOH and osmolarity adjusted to 270-280 mOsm/L. Cells were kept at -60 mV, the reversal potential for GABAergic events, or -4 mV, the reversal potential for glutamatergic events, for the recordings of mEPSCs and mIPSCs, respectively. In some experiments, picrotoxin (50 μM) and 6-cyano-7-nitroquinoxaline-2,3-dione (CNQX, 10 μM) were applied at the end of the experiment to verify that the currents were indeed GABAergic and glutamatergic, respectively. Access resistance was monitored throughout the experiments with a 5-mV negative step and was found to be constant. For current-clamp recordings, glass electrodes (6–9 MΩ) were filled with an internal solution containing the following (mM): 130 $KMeSO_4$, 5 KCl, 10 4-(2-hydroxyethyl)-1-piperazineethanesulfonic acid, 2.5 MgATP, 0.3 NaGTP, 0.2 ethyleneglycoltetraacetic acid, 10 phosphocreatine, and 0.3-0.5% biocytin, pH = 7.21. Access resistance ranged between 15- 22 MΩ, and the results were discarded if the access resistance changed by >20%. TTX, was obtained from Abcam, CNQX from Tocris and picrotoxin and kynurenic acid from Sigma.

Data were collected with a MultiClamp 700B amplifier (Molecular Devices), filtered at 2kHz, digitized (10kHz) with a Digidata 1440A (Molecular Devices) to a personal computer, and acquired using Clampex 10.1 software (PClamp, Axon Instruments, Molecular Devices). Data were analyzed and plotted in clampfit (Molecular Devices, v 10.2). Miniature currents were analyzed with Mini Analysis (Synaptosoft, version 6.0.7).

Behavior.

All behavioral tests were done with age-matched littermate of male mice, aged 8-14 weeks old. All experiments were performed according to the European Union and national recommendations for animal experimentation. The experimenter was blind to the genotype of the mice during all the tests.

Open-field. Open-field test was performed in a 40 x 40 cm square arena with an indirect illumination of 100 lux. Mouse mouvement was video-tracked using Smart 3.0 software (Panlab, Harvard apparatus) for one hour. Total distance traveled and time in center (exclusion of a 5 cm border arena), resting time, mean speed were measured. The open-field arena was cleaned and wiped with H20 and 70% ethanol between each mouse. All data shown are means +/- s.e.m. and analyzed using one way ANOVA or Kruskall-Wallis ANOVA when required. (WT : n=16 ; Het : n=15 ; KO : n=15).

Stereotyped behavior. During the first 10 min open-field test period, the number of rearings and the number of circling were measured manually. Both on-wall and off-wall rearings were counted together. An on-wall rearing event was counted when both front-paws were apposed on the wall. An off-wall rearing event was counted when both front paws had left from the floor away from the wall. A complete 360-degree turn of nose angle with respect to the body center of the mouse was counted as one circling event. All data shown are means +/- s.e.m. and analyzed using Kruskall-Wallis ANOVA. (WT : n=16 ; Het : n=15 ; KO : n=15).

Three-chamber social preference test. The test was performed as described previously (Gascon et al. 2014). The three-chamber apparatus consisted of a Plexiglas box (60 x 40 cm, each chamber being 20 x 40 cm) with removable floor and partitions dividing the box into three chambers with 5-cm openings between chambers. Test mice were housed individually the day before test. The task was carried out in five trials of 5 min each. After each trial, the

mouse was returned to his home cage for 15 min. The three-chambers apparatus was cleaned and wiped with 70% ethanol between each trial.

In the first trial, a test mouse was placed in the center of the three-chamber unit, where two empty wire cages were located in the left and right chambers to habituate the test mouse. The mouse was allowed to freely explore each chamber. The mouse was video-tracked for 5 minutes with Smart 3.0 software. In the second 5-minute session, an 8-weeks old C57Bl/6J mouse (M1) was placed randomly in one of the two wire cages to avoid any place preference. The second wire cage remained empty (E). The test mouse was placed in the center, and allowed to freely explore the chamber for 5 min. In the following two trials, the same mouse M1 was used as target, and the test mouse was placed in the center and allowed to explore each chamber. In the last 5-min session, a new 8-weeks old C57Bl/6J mouse (M2) was placed in the second wire cage. Thus, the test mouse has the choice between a familiar mouse (M1) and a new stranger mouse (M2). Time spent in each chamber and time spent within a 5-cm square proximal to each wire cage with the nose towards the cage (that we called investigation time) were measured. All data presented are means +/- s.e.m. and analysed using two-way ANOVA with Bonferroni's post hoc analysis. (WT : n=14 ; Het : n=15 ; KO : n=13).

New object recognition. The arena used for the novel object recognition test was the same used for the open-field test. The arena was cleaned and wiped with 70% ethanol between each mouse. In the habituaion session, the tested mouse was placed in the arena and allowed to explore for 10 min. Following habituation, two identical objects (50 ml orange corning tube) were placed in the opposite corners of the arena, 10 cm from the side walls. The tested mouse was placed in the center of the arena, and allowed to explore the arena for 10 min. After 24 h, one object was replaced with another novel object, which was of similar size but differ in the shape and color with the previous object (white and blue lego bricks). Then, the same mouse was placed in the center, and allowed to explore arena and two objects (a new and an "old" familiar object) for 10 min. The movement of the mice was video-

tracked with Smart 3.0 software. Time in each proximal area (nose located in a 2 cm area around the object) was measured. All data shown are means +/- s.e.m. and analyzed using Student's two-tailed, paired t-test or Wilcoxon Signed Rank Test when required. (WT : n=16; Het : n=15 ; KO : n=15).

Retrograde tracing. P28 mice under xylazine/ketamine anesthesia received stereotaxic injections of 0.3 µl of cholera toxin subunit B (CT-B, 1 mg/ml; Thermo Fisher Scientific) conjugated with Alexa Fluor 488 in the striatum (AP: +1 mm; ML: +1.8 mm; DV: −2.9 mm from dura) and conjugated with Alexa Fluor 647 in the thalamus (AP: −1.3 mm; ML: +1.15 mm; DV: −3.5 mm from dura) using Bregma coordinates. This allowed retrograde labeling of, respectively, L5 PNs (striatal injection) and L6 PNs (thalamic injection). Another group of animals were injected with Alexa Fluor 488 CT-B in motor cortex (AP: 0.6 mm; ML: 1.3 mm; DV: 0.7 mm). At 10 d after injection, animals were perfused transcardially with 4% paraformaldehyde.

RNA Isolation and library preparation. Tissue from motor plus somatosensory cortex of P28 mice were rapidly micro-dissected and frozen at -80˚C (n=3 experiments for WT, heterozygous and KO samples, 1 to 4 mice per sample). Total RNA was purified using spin columns of the RNeasy Mini Kit (Qiagen) according to manufacturer's protocol. Library preparation was made with the TruSeq mRNA-seq Stranded v2 Kit sample preparation (Illumina) according to manufacturer's instructions. One µg total RNA was used for poly(A)-selection and Elution-Fragmentation incubation time was 8 min to obtain 120-210 bp fragments. Each library was barcoded using TruSeq Single Index (Illumina). After library preparation, Agencourt AMPure XP (Beckman Coulter, Inc.) was performed for 200 to 400 bp libraries size-selection (282 nt average final library size). Each library was examined on the Bioanalyzer with High Sensitivity DNA chip (Agilent), quantified on Qubit with Qubit® dsDNA HS Assay Kit (Life Technologies), diluted to 4 nM and then pulled together at equimolar ratio.

Illumina NextSeq-500 sequencing. Sequencing was performed by the TGML Facility (INSERM U) using PolyA mRNA isolation, directional RNA-seq library preparation and the Illummina NextSeq 500 sequencer. The denaturation was performed with 5 µl of pooled libraries (4 nM) and 5 min incubation with 5 µl of fresh NaOH (0.2N) and then addition of 5 µL of fresh Tris-HCl (200 mM - pH 7), according to manufacturer's instructions. The dilution of 20 pM pooled libraries was performed with HT1 to a 1.2 pM final concentration. PhiX library as a 1% spike-in for use as a sequencing control was denatured and diluted, and 1.2 µl was added to denature and dilute pooled libraries before loading. Finally, libraries were sequenced on a high-output flow cell (400M clusters) using the NextSeq® 500/550 High Output v2 150 cycles kit (Illumina), in paired-end 75/ 75nt mode, according to manufacturer's instructions.

RNA-seq data primary analysis. 467 548 934 clusters were generated whose for 71 Gbp sequenced with 75 % >= Q30. Reads were first trimmed with sickle v1.33 (Joshin et al., 2011) (RRID:SCR_006800) with parameters –l 25 –q 20 and then aligned to mm10 using STAR v2.5.3a (Dobin et al., 2013) to produce BAM alignment files. Multi-mapped reads and reads with more than 0.08 mismatches per pair relative to read length were discarded. Transcriptome assembly were performed with Cufflinks v2.2.1 (Trapnell C. et al 2010) (RRID:SCR_014597) using the relative UCSC mm10 GTF file. For each sample Cufflinks assembles the RNA-Seq reads into individual transcripts, inferring the splicing structure of the genes and classified them as known or novel. The output GTF files from each of the Cufflinks analysis and the GTF annotation file were sent to Cuffmerge v2.2.1 (Trapnell C. et al 2010) (RRID:SCR_014597) to amalgamate them into a single unified transcript catalog.

Isoforms expression analysis from RNAseq data

Transcripts expression in fragments per kilobase of exon per million reads mapped (FPKM), were estimated and normalized with Cuffdiff v2.2.1 (Trapnell C. et al 2010) (RRID:SCR_014597) with default parameters from Cuffmerge GTF file result and alignment

files. The R package CummeRbund v2.16 (Trapnell C et all 2012) (RRID:SCR_014568) was used for data exploration and figure generation of some isoforms of interest.

Differential gene expression analysis

Gene counts were calculated with featureCounts v1.4.6-p4 (Liao Y et al., 2014) (RRID:SCR_012919) from a GTF containing known UCSC mm10 genes as well as the novel genes detected by Cufflinks (Cufflinks class code "u") and alignment files. The R package DESeq2 v1.14.1 (Love MI et al., 2014) (RRID:SCR_000154) was then used to normalize counts and detect the differentially expressed genes (FDR < 0.05). Batch effect between replicates was added in the design formula of DESeqDataSetFromMatrix function to model it in the regression step and subtract it in the differential expression test.

The RNA-Seq data discussed in this publication have been deposited in NCBI's Gene Expression Omnibus and are accessible through GEO Series accession number GSE110491 (https://www.ncbi.nlm.nih.gov/geo/query/acc.cgi?acc=GSE110491).

Gene ontology. Gene ontology enrichment was performed using all of the expressed genes as background. We used DAVID (RRID:SCR_003033) with high stringency parameters (Huang da *et al.*, 2009), and ClueGo (Cytoscape) (Bindea *et al.*, 2009) with a similar approach. DAVID adjusted p-values were used for further evaluation.

RNA-Seq statistics. We assumed that the samples were normally distributed. P-values for overlaps were calculated with binomial test using a custom made R script. P-values were subsequently adjusted for multiple comparisons using Benjamini-Hochberg FDR procedure. Two-way permutation test of 1000 was adapted to validate the overlaps. We randomized the differentially expressed gene sets by randomly selecting same number of genes from RNA-seq expressed genes and subsequently calculating the overlap P-values. Moreover we adapted a permutation test to evaluate the detected differentially expressed genes, randomizing 1000 times the RNA-seq data and recalculating the differentially expressed

genes. Analysis for RNA-seq was performed using custom made R scripts implementing functions and adapting statistical designs comprised in the libraries used. The heatmap for gene expression was performed from the gene overlap file using scripts written on R.

Statistics. All values represent the averages of independent experiments ± SEM. Statistical significance between two normally distributed groups was determined by Student's t-test using two-tailed distribution unless specified, and by Mann-Whitney test when distributions were not normal. Significance of multiple groups was determined by either one- way, or two-way, or two-way repeated measure ANOVA followed by either Bonferroni's or Tukey's post hoc test as indicated. Differences were considered to be significant if $p < 0.05$. All statistical analyses were performed with Sigmaplot 12.5 or Prism 6 (Graphpad) softwares.

Results

NeuroD2 is confined to excitatory pyramidal neurons (PNs) in the embryonic and adult cortex

We first examined NeuroD2 expression in the brain throughout development. In situ hybridizations (Allen Brain Atlas, http://www.brain-map.org/) showed that NeuroD2 mRNA is expressed in the cortical plate and hippocampus starting from E13.5 (Fig. S1a-e). In the postnatal cortex, NeuroD2 mRNA was maintained after birth, and observed in layers 2 to 6 at all ages examined (Fig. S1d-e). Quantitative RT-PCR from E14.5, E16.5 and E18.5, P7, P14 and P30 cortices showed that NeuroD2 mRNA expression reached a peak at E18.5 and then remained expressed at a constant level postnatally (Fig. S1f). At the protein level, NeuroD2 was detected embryonically (Fig. 1a, Fig. S1g) and maintained postnatally in cortical layers 2 to 6 (Fig. 1b, Fig. S1h, i). NeuroD2 protein was expressed in Ctip2-expressing PNs of layer 5 (Fig. 1c at P28; Fig. S1h at P3), and also by PNs of other layers (not shown). NeuroD2 protein was never found in Gad67-GFP^{+} inhibitory neurons (Fig. 1c, Fig. S1i) nor in glial cells (not shown). In sum, NeuroD2 is confined to PNs in all cortical layers including layer 5 and expressed lifelong, with an expression peak at E18.5.

Normal cortical layering, migration and connectivity in the absence of NeuroD2

To determine the impact of NeuroD2 deletion on gross cortical development, we first analyzed cortical architecture and laminar distribution of PNs in P30 NeuroD2 KO versus wild type (WT) mice. Global anatomy of the mutant cortex appeared unaltered as demonstrated by a normal thickness of both cortical plate and corpus callosum (Fig. 1d-e). We analyzed density and laminar distribution of PN subtypes as determined by the expression of major regulatory genes for cortical layers: Tbr1 for layer 6 cortico-thalamic (CT) neurons, Ctip2 for layer 5 pyramidal tract (PT) neurons, Satb2 for intratelencephalic (IT) neurons of layers 2/3 and 5 (Shepherd, 2013; Harris and Shepherd, 2015), and Cux1 for layer 2-3 and 4 neurons (Cubelos *et al.*, 2010). Each PN type was observed in normal amount and laminar distribution in the motor cortex (Fig. 1f-i). These parameters were also unaltered in the

somatosensory cortex (Fig. S2a-d), another area associated with ASD (Willsey *et al.*, 2013) and possibly SCZ (Reite *et al.*, 2003; Newson *et al.*, 2005), indicating that normal developmental patterning might be a general feature in the mutant cortex.

Despite normal adult lamination, delayed or accelerated radial migration can lead to neurodevelopmental disorders through abnormal maturation and connectivity of cerebral cortical PNs (Falace *et al.*, 2014). As NeuroD2 is already expressed when neurons translocate through the embryonic intermediate zone (IZ, Fig. 1a and Fig. S1g) we asked if radial migration of PN precursors is altered in mutant mice. To this aim, a red fluorescent protein (RFP) reporter plasmid was introduced into layer 5 neural progenitors by E13.5 in utero electroporation, and the distribution of RFP^+ cells analyzed 5 days later. At E18.5, in both genotypes the majority of RFP^+ cells were found in the lower cortical plate (LCP), indicating that constitutive NeuroD2 deficiency does not prevent or accelerate radial migration out of the ventricular zone (VZ) and subventricular zone (SVZ) (Fig. 1j-l).

The subtype identity of a cortical PN is determined not only by the expression of specific transcriptional regulators and the laminar position of the cell body, but also by its axonal targets (Lodato *et al.*, 2011; Rouaux and Arlotta, 2013; Ye *et al.*, 2015). Thus, we asked if axon targeting specificities are altered in NeuroD2 KO mice. We injected mice with retrograde tracers at each of three main target regions of motor cortex: the ventrolateral thalamus to label layer 6 CT neurons, the striatum to label ipsilateral PT and IT layer 5 PNs and contralateral M1 to label callosal IT neurons (Oswald *et al.*, 2013; Shepherd, 2013). In both WT and KO mice, thalamic, striatal and contralateral M1 injections retrogradely labeled preferentially layers 6, 5 and 2/3, respectively (Fig. 1m-p), indicating that axonal targeting specificities of PN subtypes is preserved in absence of NeuroD2 expression. Normal shape of the corpus callosum and of other axonal tracts after L1 immunostaining (Fig. S2e-f) confirmed the absence of axonal targeting deficits. In conclusion, NeuroD2 deficiency did not alter amount, migration, molecular and axonal targeting identities of PN subtypes.

Dendritic and synaptic phenotypes in layer 5 PNs of NeuroD2 KO mice

Chip-seq analyses of NeuroD2 binding sites in the neonatal cortex point to an enrichment in genes involved in dendritic development and synapse organization (Guner *et al.*, 2017). Furthermore, alterations in dendritic organization and spine density are specific hallmarks of ASD and SCZ (Penzes *et al.*, 2011). For these reasons, we searched for a role of NeuroD2 in dendritic and synaptic morphogenesis. As for migration analyses, we used layer 5 neurons as a model cell type relevant to ASD (Willsey *et al.*, 2013) and SCZ (Benes *et al.*, 1986). Experimentally, we obtained high-resolution access to these neurons by breeding NeuroD2 KO with the Thy1-GFP colony (line M) (Feng *et al.*, 2000; Fenelon *et al.*, 2013).

First, we analyzed dendritic length and complexity. In basal compartment, dendritic length was reduced between the 4^{th} and 5^{th} nodes away from soma in NeuroD2 KO mice (Fig. S3a,b). Furthermore, extensive 3D Sholl analysis demonstrated a significantly reduced dendritic complexity in NeuroD2 KO cells (Fig. 2a). Similarly, 3D Sholl analysis in the apical tuft showed a reduced complexity of terminal branches (Fig. 2b), while total dendritic length was unaltered (Fig. S3c-d).

Next we investigated dendritic spines, the post-synaptic elements of excitatory synapses. In P30 KO mice, spine density was significantly reduced in dendritic branches of the basal compartment (Fig. 2c,d) and even stronger in the apical tuft (Fig. 2e,f). Reduced basal spine density was mainly due to a difference in the number of thin spines (Fig. 2g), while reduced apical spine density was essentially seen for stubby spines (Fig. 2h). Morphological parameters such as head diameter, neck diameter or spine length were unaltered in NeuroD2 KO neurons (Fig. S4). Overall, we found reduced dendritic complexity and decreased spine density in NeuroD2 KO PNs, indicating that the total number of excitatory synaptic inputs might be reduced.

Electrophysiological phenotypes in layer 5 PNs of NeuroD2 KO mice

The dendritic and synaptic phenotypes prompted us to analyze physiological synaptic inputs onto GFP^+ layer 5 PNs. Although spine density was reduced the frequency of AMPAR-

mediated miniature excitatory post-synaptic currents (mEPSC) was not significantly affected (Fig. 3a,b). This absence of phenotype can be attributed to the fact that spine loss occurred mostly in apical tuft branches that are far from the soma, making a reduction in mEPSC frequency likely difficult to detect by our electrophysiological recordings. The amplitude of mEPSC was also unaltered (Fig. 3c). When measuring miniature inhibitory post-synaptic current (mIPSC) we found no significant change in frequency (Fig. 3d,e) but a significant increase in amplitude (Fig. 3d,f) in NeuroD2 KO mice.

Because NeuroD2 regulates several cell intrinsic properties of layer 2/3 neurons in the somatosensory area (Chen *et al.*, 2016), we asked if intrinsic parameters were also altered in layer 5 neurons of the motor area. Input membrane resistance was increased (Fig. 3g) and capacitance was decreased (Fig. 3h), likely reflecting the reduction in dendritic ramification shown by our 3D Sholl analysis. Interestingly, NeuroD2 KO neurons fired significantly more action potentials than WT neurons in response to depolarizing current injections (Fig. 3i,j), demonstrating increased intrinsic excitability. This increased excitability was not due to variations in action potential after-hyperpolarization as suggested for layer 2/3 neurons in these mutants (Chen *et al.*, 2016), nor to alterations in resting membrane potential or action potential threshold and amplitude (Fig. S5). Finally, we measured hyperpolarization-activated cation (Ih) currents (Benarroch, 2013) since these currents are critical integrators of synaptic integration and excitability in layer 5 PNs (Carr *et al.*, 2007; Sheets *et al.*, 2011) and are associated with both epilepsy (Benarroch, 2013) and ASD (Yi *et al.*, 2016). Compared with WT neurons, NeuroD2 KO neurons exhibited a significant increase in Ih current density (Fig. 4l,m), suggesting that NeuroD2 deficiency might affect expression or function of HCN channels. This increase in Ih current possibly represents a compensatory mechanism to reduce neuronal hyperexcitability (Benarroch, 2013).

ASD/ SCZ-like behaviors, epilepsy and hyperactivity in NeuroD2 KO and heterozygous mice

The morphological and electrophysiological phenotypes we found in layer 5 PNs of NeuroD2 KO mice have been strongly associated with ASD and SCZ (Penzes *et al.*, 2011; Han *et al.*,

2012; Harrington *et al.*, 2016; Yi *et al.*, 2016). We therefore decided to measure social behavior in NeuroD2 KO mice. We also analyzed NeuroD2 heterozygous mice, as they are more likely to represent the putative human mutations. In the novel object recognition test KO and heterozygous mice showed normal interest and memory for objects as, like WT littermates, they spent around 65% of the time investigating a novel vs familiar object (Fig. 4a-c). This result indicates that working memory is not dependent on NeuroD2. However, NeuroD2 KO mice clearly displayed abnormal social interest and social memory as demonstrated in in the three-chamber test. Unlike WT littermates, mutant mice showed no preference for the mouse-containing quadrant (Fig. 4d-f) or chamber (Fig. S6a), indicating alteration of sociability. NeuroD2 heterozygous mice behaved similar to WT in this social interaction test (Fig. 4f). In the social memory test, WT mice showed strong preference for the novel vs familiar mouse, while NeuroD2 KO and heterozygous mice did not (Fig. 4g-i for times in quadrants, Fig. S6b for times in chambers). These results indicate that sociability is altered only in KO mice while social memory/ interest is impaired in both KO and heterozygous mice.

We then looked at stereotypies, another core feature of ASD. We quantified two types of repetitive behaviors, rearing and circling, which are two accepted signs of stereotypy in mice relevant to ASD (Ryan *et al.*, 2010; Silverman *et al.*, 2010). Mutant mice showed increased rearings both at and outside cage walls while, as previously described (Olson *et al.*, 2001), heterozygous mice displayed increased circling (Fig. 4j).

Next, we investigated behaviors that show comorbidity with ASD and SCZ. A well-described comorbidity is hyperactivity (Han *et al.*, 2012; Rao and Landa, 2014; Gough and Morrison, 2016). Interestingly, this was an obvious phenotype of NeuroD2 KO mice in the open-field (Fig. 4k). NeuroD2 KO mice travelled significantly more than WT and heterozygous mice, while heterozygous displayed subtly increased locomotion compared to WTs (Fig. 4k, Fig. S6c-g). Quantification showed that KO mice had shorter resting periods and higher displacement velocities (Fig. S6d,e), confirming hyperactivity. Another comorbidity of both ASD (Canitano, 2007) and SCZ (Cascella *et al.*, 2009) is spontaneous epilepsy. We

observed spontaneous epileptic seizures in one third of NeuroD2 KO mice (Fig. 4l) during the course of the behavioral assessments. This fraction of epileptic mice is obviously an underestimate since mice were not observed continuously. Finally, we measured conflict anxiety, which requires functional integrity of the cerebral cortex (Weisstaub *et al.*, 2006) and is altered in ASD (Crawley, 2007) and SCZ (Gonzalez-Maeso *et al.*, 2008). The open field arena presents a conflict between innate drives to explore a novel environment and safety. Under brightly lit conditions, the center of the open field is aversive and potentially risk-laden, whereas exploration of the periphery provides a safer choice. We found that heterozygous and KO mice explored the center portion of the environment (as measured by the time of exploratory activity) more than their intact WT littermates did (Fig. 4m,n).

All together, our behavioral results show that NeuroD2 KO mice have behavioral defects that are reminiscent of the symptoms (altered social interest and memory, stereotypies) and comorbidities (epilepsy, hyperactivity, anxiety alterations) of ASD and SCZ in humans. NeuroD2 heterozygous mice share parts of these phenotypes, indicating that NeuroD2 is a haploinsufficient gene.

NeuroD2 target genes show a strong enrichment in voltage-sensitive ion channel activity, synapse modulation, ASD and SCZ

Since NeuroD2 is a nuclear transcription factor, we sought to identify differentially expressed genes in KO mice and to ask which proportion might regulate synaptic transmission, neuronal cell intrinsic excitability and/or behaviors relevant to neuropsychiatric disorders. We analyzed differentially expressed genes in the cerebral cortex of KO versus WT mice at P28. We micro-dissected ASD and SCZ-relevant cortical tissue encompassing motor and somatosensory areas (Willsey *et al.*, 2013) (Fig. 5a). Deep sequencing of polyA-enriched mRNAs (RNA-seq) identified 263 differentially expressed genes, including 184 genes with a decreased expression and 79 genes with an increased expression (70% versus 30%,

respectively). No particular bias towards a specific cortical layer was found among the differentially expressed genes (Fig. 5b and Fig. S8).

Gene ontology (GO) analysis with ClueGO (Bindea *et al.*, 2009) and DAVID (Huang da *et al.*, 2009) functional annotation tools both revealed that genes with reduced expression in KO mice were most significantly enriched for the following biological processes: voltage-gated ion channel activity, cell projection morphogenesis, chemical synaptic transmission and neuronal action potential (Fig. 5c and Fig. S7 for ClueGO; Table 1 and Supplementary file 1 for DAVID). Differentially expressed genes coding for voltage sensitive ion channels included the sodium channels Scn1a, Scn4b and Scn8a, the potassium channels Kcnh1, Kcnq5, Kcnj6, Kcna5, Kcnv1 and Kcnk4, Kcnma1 and the calcium channels Cacna1c and Cacna2d2 (Fig. 5d). Dysregulation of one or more of these channels is likely involved in the hyperexcitability of layer 5 NeuroD2 KO PNs. Analysis of genes up-regulated in NeuroD2 KO mice revealed a significant enrichment for multicellular organismal response to stress (Fig. S7, Table 1), which since NeuroD2 is a putatively pure transactivator might be at least in part a homeostatic consequence of initial cell dysfunction induced by downregulated genes.

Among downregulated genes, a good candidate for spine density regulation is the glucocorticoid receptor, Nr3c1, because it is a critical regulator of spine development in layer 5 neuron apical dendrites, which is where spine density is most affected in NeuroD2 KO neurons (Fig. 2). Another candidate for this phenotype is the synaptome gene Syne1 (Fig. 5e) because it encodes many actin-binding protein isoforms of which only one, called CPG2, is brain-specific and regulates synapse formation (Packard *et al.*, 2015). Isoform expression analysis showed that CPG2 is the main Syne1 isoform in WT cortex and with the strongest downregulation in NeuroD2 KO mice (Fig. S9), confirming that CPG downregulation could be causally linked with spine defects in mutant neurons. Concerning increased Ih current density in mutant neurons (Fig. 3l,m), a likely candidate gene that comes out of our RNA-seq screen is Trip8b (Supplementary File 1), a known brain-specific auxiliary subunit of HCN1 and critical regulator of the membrane localization and expression of HCN1 channels and thus of Ih current density (Santoro *et al.*, 2009; Piskorowski *et al.*, 2011). Concerning

increased mIPSC amplitude (Fig. 3f) however, we found no dysregulated gene directly linked with postsynaptic inhibitory signaling (Jacob *et al.*, 2008).

To further characterize the NeuroD2 KO differentially expressed genes, we compared our dysregulated gene list with the recently updated risk genes from the Simons Foundation Autism Research Initiative (Pereanu *et al.*, 2017) (SFARI database, 859 genes), mRNAs associated with FMRP (Darnell *et al.*, 2011) (842 genes), ID-associated genes from multiple sources (Inlow and Restifo, 2004; Ropers, 2008; van Bokhoven, 2011; Lubs *et al.*, 2012), SCZ-associated genes ((Schizophrenia Working Group of the Psychiatric Genomics, 2014) and OMIM with "*schizophrenia"* as a keyword, 196 genes) and synaptic-associated genes (Pirooznia *et al.*, 2012) (SynaptomeDB, 1876 genes). Strikingly, among the 263 differentially expressed genes, 39 were synaptome-related genes, 35 were associated with ASD, 37 with FMRP and 6 with SCZ (Fig. 5f,g). Statistically, these proportions of synaptome, ASD, FMRP and SCZ-related genes were very considerably higher than what a random sampling would produce (Fig. 5e for binomial test, but hypergeometric test gave comparable significance). ASD/ SCZ genes included the Dravet syndrome gene Scn1a and the Timothy syndrome gene Cacna1c that both are voltage-gated ion channels, but also Grin2b, Htr2a, Pcdh9 and other well described ASD genes (Fig. 5h). In contrast, the proportion of intellectual disability genes among the differentially expressed genes was not significantly higher than expected by chance (Fig. 5e). Using quantitative PCR (qPCR) or immunohistochemistry, we validated dysregulation of several voltage-gated ion channels and factors related to neuropsychiatric disorders in NeuroD2 KO mice (Fig. S10).

Overall, our RNAseq data analysis suggests that NeuroD2, either directly or indirectly, influences a large, complex gene expression program that controls neuronal and synapse development, and numerous syndromic and idiopathic ASD and SCZ-linked genes.

Discussion

By analyzing the development of the cerebral cortex in NeuroD2 KO mice and focusing on layer 5 of the ASD/ SCZ-associated (Benes *et al.*, 1986; Willsey *et al.*, 2013) motor area, we find that NeuroD2 KO PNs exhibit molecular, structural, electrophysiological and behavioral alterations that are highly relevant to ASD and SCZ. NeuroD2 deficiency does not alter migration, subtype specification, layer position and axonal targeting identity of PNs, but reduces spine density, increases cell intrinsic excitability and mIPSC amplitude, and alters the expression of a high fraction of known ASD and SCZ genes. At the behavioral level, NeuroD2 deficiency decreases sociability and social memory, increases stereotypies and induces epilepsy and hyperactivity, two ASD/ SCZ-comorbid behaviors. These extensive analyses strongly support the potential implication of NeuroD2 mutations in human neuropsychiatric disorders.

NeuroD2 as a synapse/ excitability regulating transcription factor

Previous Chip-seq studies have found that NeuroD2 is able to bind many genetic loci (Fong *et al.*, 2012; Bayam *et al.*, 2015). Moreover, NeuroD2 is highly expressed in PNs, from postmitotic neural progenitors in the subventricular zone to mature neurons. Thus, NeuroD2 functional targets were initially thought to be likely involved in many biological processes throughout neural development in the neocortex. This is exemplified by a Chip-seq analysis in the embryonic cortex that revealed an enrichment of migration-related genes in NeuroD2 binding targets (Bayam *et al.*, 2015).

However, in juvenile mice (P28), our gene expression analysis reveals that NeuroD2 absence is mainly impacting voltage-sensitive ion channels, synaptic and ASD/ SCZ genes. Moreover, our extensive phenotypic analysis indicates that more than a generic pro-neuronal gene, NeuroD2 could be a regulator of synaptic integration and/ or excitability in neurons. It is striking that we did not observe any obvious axonal growth defects in mutant mice, strongly contrasting with the phenotype of NeuroD2/NeuroD6 double mutant animals (Bormuth *et al.*, 2013). A possible explanation resides in the functional redundancy with other

NeuroD family members during neuronal development. In this context, it seems plausible that synaptic regulation and/ or excitability regulations are specific function(s) of NeuroD2 among other NeuroDs. Indeed, NeuroD2 is the only member of the NeuroD family that has been linked to synaptic integration and maturation (Ince-Dunn *et al.*, 2006; Wilke *et al.*, 2012; Chen *et al.*, 2016; Chen and Hall, 2017), indicating that functional redundancy may not hold true for regulation of synaptic integration/ excitability.

Initial defects and homeostatic compensation in complex cortical phenotypes

Whether regulation of synaptic integration and of intrinsic excitability are independent consequences of a NeuroD2 effect or whether one is a homeostatic consequence of the other remains an open question. This problem is in line with recent theories pointing the difficulty to separate initial deficits from homeostatic compensation in the study of syndromic ASD models (Nelson and Valakh, 2015). At the electrophysiological level, Chen et al. (2016) found that layer 2/3 PNs of the somatosensory area receive less excitatory and inhibitory inputs after NeuroD2 deletion, as the frequencies of both mEPSCs and mIPSCs were reduced (Chen *et al.*, 2016). This striking difference with our electrophysiological data showing normal mEPSCs and increased mIPSC amplitude suggests that a genetic mutation can induce different and even opposite cellular phenotypes in different cortical areas/layers. Also, these complex region-dependent phenotypes constitute another demonstration that initial defects and homeostatic compensation phenotypes cannot be discriminated when studying constitutive mutations. In the future, conditional deletion and the use of neuron subtype specific driver mice should allow separating initial from compensatory defects in different brain areas to better elucidate the mechanisms responsible for complex cortical phenotypes in neuropsychiatric disorders.

Associating NeuroD2 transcriptional targets with cellular and behavioral phenotypes: insights from our RNA-seq data

Literature-based screening of our gene list indicated that dysregulation of the Syne1 splice variant CPG and the glucocorticoid receptor Nr3c1 might be involved in spine density deficits.

Importantly, Nr3c1 regulates spine density in apical tuft dendrites of layer 5 neurons (Liston and Gan, 2011), precisely where we found the strongest phenotype. Chronic and short-term stresses both preferentially affect apical tuft dendrites and spines through glucocorticoid binding to Nr3c1 in layer 1 (Brown *et al.*, 2005), which induces a ligand-dependent transcription factor activity of Nr3c1 that is NeuroD2-dependent. Indeed, a recent study showed that NeuroD2 acts as a critical cofactor for Nr3c1 transactivation at least in vitro (van Weert *et al.*, 2017). Together with our novel finding that NeuroD2 is also a transcriptional inducer of Nr3c1 expression, these evidences suggest that NeuroD2 is a critical regulator of stress-induced synaptic integration and possibly plasticity in layer 5 cortical neurons. This hypothesis is corroborated by the reported fearless behavior of NeuroD2 KO mice (Lin *et al.*, 2005) and by their reduced cortical-dependent conflict anxiety shown here.

Concerning locomotor hyperactivity and spontaneous epilepsy in NeuroD2 KO mice, best candidates to be found among the 13 differentially expressed voltage-gated ion channels are the layer 5 enriched potassium channel Kcnq5 (Molyneaux *et al.*, 2015; Lehman *et al.*, 2017) (Allen Brain Atlas) and the Scn8a sodium channel that regulates dendritic excitability in cortical PNs (Lorincz and Nusser, 2010).

The increased mIPSC amplitude in NeuroD2 KO neurons primarily suggests increased post-synaptic expression or trafficking of GABA-A receptors; however we could not find any obvious differentially expressed gene that could account for this phenotype. Alternatively, the increased mIPSC amplitude might be a consequence of the changes in electrotonic, passive membrane properties due to reduced dendritic complexity and associated increased input resistance rather than to a genuine change in inhibitory synaptic transmission.

Concerning increased Ih current in NeuroD2 KO neurons, downregulation of Trip8b, a critical regulator of the membrane localization and expression of HCN1 channels (Santoro *et al.*, 2009; Piskorowski *et al.*, 2011) is a likely candidate. Independently of its mechanism, increased Ih currents tend to decrease intrinsic neuronal excitability, suggesting that this phenotype is not part of initial defects but instead might represent a compensatory mechanism to reduce neuronal hyperexcitability (Benarroch, 2013).

Relevance for psychiatric disorders (ASD/ SCZ)

NeuroD2 locus has been associated with SCZ and ASD in humans. Indeed, a recent study has demonstrated an association between rare polymorphisms in NeuroD2 and SCZ (Spellmann *et al.*, 2017). Furthermore, NeuroD2 mRNA contains a high-confidence target site for the well-described SCZ-related microRNA miR-137 (Cross-Disorder Group of the Psychiatric Genomics, 2013; Ripke *et al.*, 2013) according to miRNA prediction programs (TargetScan, miRanda). Third, the main transcriptional cofactor of NeuroD2 is the schizophrenia gene TCF4 (Amiel *et al.*, 2007; Brockschmidt *et al.*, 2007; Zweier *et al.*, 2007; Ravanpay and Olson, 2008). Together, these evidences reinforce the hypothesis that NeuroD2 might be involved in SCZ in humans. It is also interesting to note that copy number variations encompassing the NeuroD2 locus have been associated with ASD (DECIPHER, https://decipher.sanger.ac.uk/). Moreover, a machine-learning based approach that compares candidate gene co-expression and co-function with already-known ASD genes to find new ASD genes ranked NeuroD2 98th out of 25,825 genes (Krishnan *et al.*, 2016) (Fig. S9) as a good candidate for ASD. Comforting these results, for the first time we show compelling evidence that NeuroD2 is necessary for the development of normal social behavior in mice. Although the behavioral alterations we observed in NeuroD2 KO mice are not necessarily related to ASD or SCZ, the strong disruption of social interest and memory, the latter being also true for heterozygote mice, supports the involvement of NeuroD2 in neuropsychiatric disorders. Interestingly, social memory impairment (Piskorowski *et al.*,

2016) and hyperactivity (van den Buuse, 2010) are typical features of SCZ and SCZ mouse models.

Conclusions and Perspectives

Our findings of cerebral cortex-related synaptic, physiological and behavioral alterations in NeuroD2 KO mice, together with genetic associations with psychiatric disorders in humans, highlight the potential of NeuroD2 as a synaptopathy gene.

There are evidences suggesting a link between NeuroD2 and neuronal activity. Indeed NeuroD2 transactivator activity is increased by neuronal depolarization (Ince-Dunn *et al.*, 2006), and NeuroD2 expression is regulated by NMDAR activation (Chen and Hall, 2017). In this context, it will be of great interest to test whether and how NeuroD2 can be involved in experience-dependent synaptic plasticity, and if yes how it relates to neuropsychiatric disorders in general.

Acknowledgements:

This work was supported by the Agence Nationale de la Recherche (ANR-13-JSV4-0006 to A.d.C.), the Fondation Pour la Recherche sur le Cerveau (to A.d.C.) and the Fondation Lejeune (to A.d.C.). Highthroughput sequencing was performed at the TGML Platform, supported by grants from Inserm, GIS IBiSA, Aix-Marseille Université, and ANR-10-INBS-0009-10.

References:

Amiel J, Rio M, de Pontual L, Redon R, Malan V, Boddaert N*, et al.* Mutations in TCF4, encoding a class I basic helix-loop-helix transcription factor, are responsible for Pitt-Hopkins syndrome, a severe epileptic encephalopathy associated with autonomic dysfunction. American journal of human genetics 2007; 80(5): 988-93.

Bayam E, Sahin GS, Guzelsoy G, Guner G, Kabakcioglu A, Ince-Dunn G. Genome-wide target analysis of NEUROD2 provides new insights into regulation of cortical projection neuron migration and differentiation. BMC Genomics 2015; 16(1): 681.

Benarroch EE. HCN channels: function and clinical implications. Neurology 2013; 80(3): 304-10.

Benes FM, Davidson J, Bird ED. Quantitative cytoarchitectural studies of the cerebral cortex of schizophrenics. Arch Gen Psychiatry 1986; 43(1): 31-5.

Bindea G, Mlecnik B, Hackl H, Charoentong P, Tosolini M, Kirilovsky A*, et al.* ClueGO: a Cytoscape plug-in to decipher functionally grouped gene ontology and pathway annotation networks. Bioinformatics 2009; 25(8): 1091-3.

Bormuth I, Yan K, Yonemasu T, Gummert M, Zhang M, Wichert S*, et al.* Neuronal basic helix-loop-helix proteins Neurod2/6 regulate cortical commissure formation before midline interactions. J Neurosci 2013; 33(2): 641-51.

Brockschmidt A, Todt U, Ryu S, Hoischen A, Landwehr C, Birnbaum S*, et al.* Severe mental retardation with breathing abnormalities (Pitt-Hopkins syndrome) is caused by haploinsufficiency of the neuronal bHLH transcription factor TCF4. Hum Mol Genet 2007; 16(12): 1488-94.

Brown SM, Henning S, Wellman CL. Mild, short-term stress alters dendritic morphology in rat medial prefrontal cortex. Cereb Cortex 2005; 15(11): 1714-22.

Canitano R. Epilepsy in autism spectrum disorders. Eur Child Adolesc Psychiatry 2007; 16(1): 61-6.

Carr DB, Andrews GD, Glen WB, Lavin A. alpha2-Noradrenergic receptors activation enhances excitability and synaptic integration in rat prefrontal cortex PNs via inhibition of HCN currents. J Physiol 2007; 584(Pt 2): 437-50.

Cascella NG, Schretlen DJ, Sawa A. Schizophrenia and epilepsy: is there a shared susceptibility? Neurosci Res 2009; 63(4): 227-35.

Chen F, Hall BJ. Synaptic activity suppresses expression of neurogenic differentiation factor 2 in an NMDA receptor-dependent manner. Synapse 2017; 71(9).

Chen F, Moran JT, Zhang Y, Ates KM, Yu D, Schrader LA*, et al.* The transcription factor NeuroD2 coordinates synaptic innervation and cell intrinsic properties to control excitability of cortical PNs. J Physiol 2016; 594(13): 3729-44.

Crawley JN. Mouse behavioral assays relevant to the symptoms of autism. Brain Pathol 2007; 17(4): 448-59.

Cross-Disorder Group of the Psychiatric Genomics C. Identification of risk loci with shared effects on five major psychiatric disorders: a genome-wide analysis. Lancet 2013; 381(9875): 1371-9.

Cubelos B, Sebastian-Serrano A, Beccari L, Calcagnotto ME, Cisneros E, Kim S*, et al.* Cux1 and Cux2 regulate dendritic branching, spine morphology, and synapses of the upper layer neurons of the cortex. Neuron 2010; 66(4): 523-35.

Darnell JC, Van Driesche SJ, Zhang C, Hung KY, Mele A, Fraser CE*, et al.* FMRP stalls ribosomal translocation on mRNAs linked to synaptic function and autism. Cell 2011; 146(2): 247-61.

de Chevigny A, Core N, Follert P, Gaudin M, Barbry P, Beclin C*, et al.* miR-7a regulation of Pax6 controls spatial origin of forebrain dopaminergic neurons. Nature neuroscience 2012; 15(8): 1120-6.

Falace A, Buhler E, Fadda M, Watrin F, Lippiello P, Pallesi-Pocachard E*, et al.* TBC1D24 regulates neuronal migration and maturation through modulation of the ARF6-dependent pathway. Proceedings of the National Academy of Sciences of the United States of America 2014; 111(6): 2337-42.

Fenelon K, Xu B, Lai CS, Mukai J, Markx S, Stark KL*, et al.* The pattern of cortical dysfunction in a mouse model of a schizophrenia-related microdeletion. J Neurosci 2013; 33(37): 14825-39.

Feng G, Mellor RH, Bernstein M, Keller-Peck C, Nguyen QT, Wallace M*, et al.* Imaging neuronal subsets in transgenic mice expressing multiple spectral variants of GFP. Neuron 2000; 28(1): 41-51.

Fong AP, Yao Z, Zhong JW, Cao Y, Ruzzo WL, Gentleman RC*, et al.* Genetic and epigenetic determinants of neurogenesis and myogenesis. Dev Cell 2012; 22(4): 721-35.

Gonzalez-Maeso J, Ang RL, Yuen T, Chan P, Weisstaub NV, Lopez-Gimenez JF*, et al.* Identification of a serotonin/glutamate receptor complex implicated in psychosis. Nature 2008; 452(7183): 93-7.

Gough A, Morrison J. Managing the comorbidity of schizophrenia and ADHD. J Psychiatry Neurosci 2016; 41(5): E79-80.

Guner G, Guzelsoy G, Isleyen FS, Sahin GS, Akkaya C, Bayam E*, et al.* NEUROD2 Regulates Stim1 Expression and Store-Operated Calcium Entry in Cortical Neurons. eNeuro 2017; 4(1).

Han S, Tai C, Westenbroek RE, Yu FH, Cheah CS, Potter GB*, et al.* Autistic-like behaviour in Scn1a+/- mice and rescue by enhanced GABA-mediated neurotransmission. Nature 2012; 489(7416): 385-90.

Harrington AJ, Raissi A, Rajkovich K, Berto S, Kumar J, Molinaro G*, et al.* MEF2C regulates cortical inhibitory and excitatory synapses and behaviors relevant to neurodevelopmental disorders. Elife 2016; 5.

Harris KD, Shepherd GM. The neocortical circuit: themes and variations. Nature neuroscience 2015; 18(2): 170-81.

Huang da W, Sherman BT, Lempicki RA. Systematic and integrative analysis of large gene lists using DAVID bioinformatics resources. Nat Protoc 2009; 4(1): 44-57.

Ince-Dunn G, Hall BJ, Hu SC, Ripley B, Huganir RL, Olson JM*, et al.* Regulation of thalamocortical patterning and synaptic maturation by NeuroD2. Neuron 2006; 49(5): 683-95.

Inlow JK, Restifo LL. Molecular and comparative genetics of mental retardation. Genetics 2004; 166(2): 835-81.

Jacob TC, Moss SJ, Jurd R. GABA(A) receptor trafficking and its role in the dynamic modulation of neuronal inhibition. Nature reviews Neuroscience 2008; 9(5): 331-43.

Krishnan A, Zhang R, Yao V, Theesfeld CL, Wong AK, Tadych A*, et al.* Genome-wide prediction and functional characterization of the genetic basis of autism spectrum disorder. Nature neuroscience 2016; 19(11): 1454-62.

Lee JE, Hollenberg SM, Snider L, Turner DL, Lipnick N, Weintraub H. Conversion of Xenopus ectoderm into neurons by NeuroD, a basic helix-loop-helix protein. Science 1995; 268(5212): 836-44.

Lehman A, Thouta S, Mancini GMS, Naidu S, van Slegtenhorst M, McWalter K*, et al.* Loss-of-Function and Gain-of-Function Mutations in KCNQ5 Cause Intellectual Disability or Epileptic Encephalopathy. American journal of human genetics 2017; 101(1): 65-74.

Lin CH, Hansen S, Wang Z, Storm DR, Tapscott SJ, Olson JM. The dosage of the neuroD2 transcription factor regulates amygdala development and emotional learning. Proceedings of the National Academy of Sciences of the United States of America 2005; 102(41): 14877-82.

Liston C, Gan WB. Glucocorticoids are critical regulators of dendritic spine development and plasticity in vivo. Proceedings of the National Academy of Sciences of the United States of America 2011; 108(38): 16074-9.

Lodato S, Rouaux C, Quast KB, Jantrachotechatchawan C, Studer M, Hensch TK*, et al.* Excitatory projection neuron subtypes control the distribution of local inhibitory interneurons in the cerebral cortex. Neuron 2011; 69(4): 763-79.

Lorincz A, Nusser Z. Molecular identity of dendritic voltage-gated sodium channels. Science 2010; 328(5980): 906-9.

Lubs HA, Stevenson RE, Schwartz CE. Fragile X and X-linked intellectual disability: four decades of discovery. American journal of human genetics 2012; 90(4): 579-90.

McCormick MB, Tamimi RM, Snider L, Asakura A, Bergstrom D, Tapscott SJ. NeuroD2 and neuroD3: distinct expression patterns and transcriptional activation potentials within the neuroD gene family. Mol Cell Biol 1996; 16(10): 5792-800.

Molyneaux BJ, Goff LA, Brettler AC, Chen HH, Hrvatin S, Rinn JL*, et al.* DeCoN: genome-wide analysis of in vivo transcriptional dynamics during pyramidal neuron fate selection in neocortex. Neuron 2015; 85(2): 275-88.

Nelson SB, Valakh V. Excitatory/Inhibitory Balance and Circuit Homeostasis in Autism Spectrum Disorders. Neuron 2015; 87(4): 684-98.

Newson P, Lynch-Frame A, Roach R, Bennett S, Carr V, Chahl LA. Intrinsic sensory deprivation induced by neonatal capsaicin treatment induces changes in rat brain and behaviour of possible relevance to schizophrenia. Br J Pharmacol 2005; 146(3): 408-18.

Olson JM, Asakura A, Snider L, Hawkes R, Strand A, Stoeck J*, et al.* NeuroD2 is necessary for development and survival of central nervous system neurons. Dev Biol 2001; 234(1): 174-87.

Oswald MJ, Tantirigama ML, Sonntag I, Hughes SM, Empson RM. Diversity of layer 5 projection neurons in the mouse motor cortex. Front Cell Neurosci 2013; 7: 174.

Packard M, Jokhi V, Ding B, Ruiz-Canada C, Ashley J, Budnik V. Nucleus to Synapse Nesprin1 Railroad Tracks Direct Synapse Maturation through RNA Localization. Neuron 2015; 86(4): 1015-28.

Penzes P, Cahill ME, Jones KA, VanLeeuwen JE, Woolfrey KM. Dendritic spine pathology in neuropsychiatric disorders. Nature neuroscience 2011; 14(3): 285-93.

Pereanu W, Larsen EC, Das I, Estevez MA, Sarkar AA, Spring-Pearson S*, et al.* AutDB: a platform to decode the genetic architecture of autism. Nucleic Acids Res 2017.

Pirooznia M, Wang T, Avramopoulos D, Valle D, Thomas G, Huganir RL*, et al.* SynaptomeDB: an ontology-based knowledgebase for synaptic genes. Bioinformatics 2012; 28(6): 897-9.

Piskorowski R, Santoro B, Siegelbaum SA. TRIP8b splice forms act in concert to regulate the localization and expression of HCN1 channels in CA1 PNs. Neuron 2011; 70(3): 495-509.

Piskorowski RA, Nasrallah K, Diamantopoulou A, Mukai J, Hassan SI, Siegelbaum SA*, et al.* Age-Dependent Specific Changes in Area CA2 of the Hippocampus and Social Memory Deficit in a Mouse Model of the 22q11.2 Deletion Syndrome. Neuron 2016; 89(1): 163-76.

Rao PA, Landa RJ. Association between severity of behavioral phenotype and comorbid attention deficit hyperactivity disorder symptoms in children with autism spectrum disorders. Autism 2014; 18(3): 272-80.

Ravanpay AC, Olson JM. E protein dosage influences brain development more than family member identity. J Neurosci Res 2008; 86(7): 1472-81.

Reite M, Teale P, Rojas DC, Benkers TL, Carlson J. Anomalous somatosensory cortical localization in schizophrenia. Am J Psychiatry 2003; 160(12): 2148-53.

Ripke S, O'Dushlaine C, Chambert K, Moran JL, Kahler AK, Akterin S*, et al.* Genome-wide association analysis identifies 13 new risk loci for schizophrenia. Nat Genet 2013; 45(10): 1150-9.

Ropers HH. Genetics of intellectual disability. Curr Opin Genet Dev 2008; 18(3): 241-50.

Rouaux C, Arlotta P. Direct lineage reprogramming of post-mitotic callosal neurons into corticofugal neurons in vivo. Nat Cell Biol 2013; 15(2): 214-21.

Rubenstein JL, Merzenich MM. Model of autism: increased ratio of excitation/inhibition in key neural systems. Genes Brain Behav 2003; 2(5): 255-67.

Ryan BC, Young NB, Crawley JN, Bodfish JW, Moy SS. Social deficits, stereotypy and early emergence of repetitive behavior in the C58/J inbred mouse strain. Behav Brain Res 2010; 208(1): 178-88.

Santoro B, Piskorowski RA, Pian P, Hu L, Liu H, Siegelbaum SA. TRIP8b splice variants form a family of auxiliary subunits that regulate gating and trafficking of HCN channels in the brain. Neuron 2009; 62(6): 802-13.

Schizophrenia Working Group of the Psychiatric Genomics C. Biological insights from 108 schizophrenia-associated genetic loci. Nature 2014; 511(7510): 421-7.

Sheets PL, Suter BA, Kiritani T, Chan CS, Surmeier DJ, Shepherd GM. Corticospinal-specific HCN expression in mouse motor cortex: I(h)-dependent synaptic integration as a candidate microcircuit mechanism involved in motor control. J Neurophysiol 2011; 106(5): 2216-31.

Shepherd GM. Corticostriatal connectivity and its role in disease. Nature reviews Neuroscience 2013; 14(4): 278-91.

Silverman JL, Yang M, Lord C, Crawley JN. Behavioural phenotyping assays for mouse models of autism. Nature reviews Neuroscience 2010; 11(7): 490-502.

Spellmann I, Riedel M, Stadtler J, Zill P, Obermeier M, Cerovecki A*, et al.* Associations of NEUROD2 polymorphisms and change of cognitive dysfunctions in schizophrenia and schizoaffective disorder after eight weeks of antipsychotic treatment. Cogn Neuropsychiatry 2017; 22(4): 280-97.

van Bokhoven H. Genetic and epigenetic networks in intellectual disabilities. Annu Rev Genet 2011; 45: 81-104.

van den Buuse M. Modeling the positive symptoms of schizophrenia in genetically modified mice: pharmacology and methodology aspects. Schizophr Bull 2010; 36(2): 246-70.

van Weert L, Buurstede JC, Mahfouz A, Braakhuis PSM, Polman JAE, Sips HCM*, et al.* NeuroD Factors Discriminate Mineralocorticoid From Glucocorticoid Receptor DNA Binding in the Male Rat Brain. Endocrinology 2017; 158(5): 1511-22.

Weisstaub NV, Zhou M, Lira A, Lambe E, Gonzalez-Maeso J, Hornung JP*, et al.* Cortical 5-HT2A receptor signaling modulates anxiety-like behaviors in mice. Science 2006; 313(5786): 536-40.

Wilke SA, Hall BJ, Antonios JK, Denardo LA, Otto S, Yuan B*, et al.* NeuroD2 regulates the development of hippocampal mossy fiber synapses. Neural Dev 2012; 7: 9.

Willsey AJ, Sanders SJ, Li M, Dong S, Tebbenkamp AT, Muhle RA*, et al.* Coexpression networks implicate human midfetal deep cortical projection neurons in the pathogenesis of autism. Cell 2013; 155(5): 997-1007.

Yang Y, Kim AH, Yamada T, Wu B, Bilimoria PM, Ikeuchi Y*, et al.* A Cdc20-APC ubiquitin signaling pathway regulates presynaptic differentiation. Science 2009; 326(5952): 575-8.

Ye Z, Mostajo-Radji MA, Brown JR, Rouaux C, Tomassy GS, Hensch TK*, et al.* Instructing Perisomatic Inhibition by Direct Lineage Reprogramming of Neocortical Projection Neurons. Neuron 2015; 88(3): 475-83.

Yi F, Danko T, Botelho SC, Patzke C, Pak C, Wernig M*, et al.* Autism-associated SHANK3 haploinsufficiency causes Ih channelopathy in human neurons. Science 2016; 352(6286): aaf2669.

Zoghbi HY, Bear MF. Synaptic dysfunction in neurodevelopmental disorders associated with autism and intellectual disabilities. Cold Spring Harbor perspectives in biology 2012; 4(3).

Zweier C, Peippo MM, Hoyer J, Sousa S, Bottani A, Clayton-Smith J*, et al.* Haploinsufficiency of TCF4 causes syndromal mental retardation with intermittent hyperventilation (Pitt-Hopkins syndrome). American journal of human genetics 2007; 80(5): 994-1001.

Table 1: Gene ontology with DAVID.

	Term	Count	PValue	Benjamini	FDR
GLOBAL	Voltage-gated ion channel activity	13	1.91E-06	0.002	0.003
GLOBAL	Signal transduction	30	7.34E-06	0.005	0.012
GLOBAL	Chemical synaptic transmission	11	3.06E-05	0.013	0.050
GLOBAL	Neuronal action potential	6	3.71E-05	0.012	0.061
GLOBAL	Intracellular signal transduction	18	5.25E-05	0.014	0.086
GLOBAL	Axon guidance	11	5.99E-05	0.013	0.098
GLOBAL	Regulation of membrane potential	8	2.13E-04	0.039	0.347
GLOBAL	Neuromuscular junction development	6	2.85E-04	0.045	0.464
GLOBAL	Adult walking behavior	6	3.29E-04	0.046	0.536
GLOBAL	Nervous system development	15	9.69E-04	0.118	1.570
GLOBAL	Long-term synaptic potentiation	6	9.99E-04	0.111	1.618
DOWN	Voltage-gated ion channel activity	11	4.27E-06	0.004	0.007
DOWN	Axon guidance	10	1.75E-05	0.008	0.027
DOWN	Neuronal action potential	5	1.40E-04	0.042	0.218
DOWN	Regulation of membrane potential	7	1.91E-04	0.043	0.298
DOWN	Ion transport	15	2.68E-04	0.048	0.419
DOWN	Nervous system development	13	3.19E-04	0.048	0.498
DOWN	Chemical synaptic transmission	8	4.53E-04	0.058	0.705
DOWN	Signal transduction	20	5.17E-04	0.058	0.805
UP	Regulation of cell growth	4	0.002	0.701	2.977
UP	Insulin secretion	3	0.006	0.851	9.085
UP	Signal transduction	10	0.010	0.858	13.619
UP	Cell adhesion	7	0.012	0.824	15.969
UP	Positive regulation of stress fiber assembly	3	0.016	0.848	20.979

Footnote: GLOBAL: all differentially expressed genes. DOWN: down-regulated genes. UP: up-regulated genes. FDR: False Discovery Rate.

Most appropriate position for Table 1: after or in the middle of the Result paragraph subheaded **"**NeuroD2 target genes show a strong enrichment in voltage-sensitive ion channel activity, synapse modulation, ASD and SCZ".

Supplementary File 1: List of differentially expressed (DEX) genes as revealed by RNA-seq.

Figure 1: Normal migration, laminar organization and axonal targeting of PNs in NeuroD2 KO mice. (a-c) Expression of NeuroD2 in PNs during cortical development. NeuroD2 protein was detected in the intermediate zone and cortical plate at E16.5 (a), and in cortical layers 2 to 6 at P28 (b). (c) NeuroD2 protein co-localized with the layer 5 marker Ctip2 but not with Gad67-GFP. (d,e) Cortical and callosal widths were unaltered in NeuroD2 KO mice. (f-i) Density and laminar distribution of Tbr1+ (g), Ctip2+ (h), Satb2+ (i) and Cux1+ cells (j) in a column of the motor cortex were unaltered in NeuroD2 KO mice.(j-l) Migration of pyramidal neuron precursors is unaffected in NeuroD2 KO mice. RFP was electroporated in layer 5 motor cortex neurons and laminar distribution of RFP+ cells analyzed at E18.5 (j). (k) Representative images of RFP+ cells in WT and KO. (l) Quantification revealed an unaltered laminar distribution in KO mice. (m-p) Axonal targeting of pyramidal neuron subtypes. Fluorescent retrograde cholera toxin beta striatal (n), thalamic (o) and contralateral M1 including layer 2/3 and 5 cells injections led to similar distribution of retrogradely labeled somata in the ipsilateral motor cortex. CP, cortical plate;, IZ, intermediate zone; MZ, marginal zone; M1, primary motor cortex; S1, primary somatosensory cortex. Scale bars: a, 200 µm; b, 250 µm; c, 10 µm; f, g, h, i, 200 µm ;k, 100 µm; m, 100 µm. Data are means ± SEM. Number of animals or slices/ animals [for (n) and (o)] analyzed are shown in bars or parentheses. Statistical significance was evaluated by two-tailed Student's t test [bar graphs in (d)-(i)] or two-way repeated measure ANOVA [(l), (n) and (o)].

Figure 2: Dendritic and spine phenotypes in layer 5 PNs of NeuroD2 KO mice. (a,b) Sholl analysis of basal (a) and apical (b) dendrites demonstrated a slightly reduced complexity in NeuroD2 KO neurons. (c-f) Spine density reduction in NeuroD2 KO mice. (c,d) Spine density was reduced in basal dendrites. (c) Representative photomicrographs of basal dendritic branches in WT and KO mice, (d) quantification of spine density. (e,f) Reduced spine density in apical tuft dendrites. (e) Images and (f) histogram of quantification. (g,h) Spine subtypes density in basal and apical compartments. (g) Thin spine were reduced in basal dendrites. (h) Stubby spines exhibited reduced density in apical tuft dendrites. Scale

bars: a, ; c,e, . Data are means ± SEM. Number of dendrites/ animals analyzed are shown in bars or parentheses. Statistical significance was evaluated by two-tailed Student's t test [(d), (f), (g) and (h)] or two-way repeated measure ANOVA followed by Bonferroni's post hoc test [(a) and (b)].

Figure 3: Electrophysiological phenotypes in layer 5 PNs of NeuroD2 KO mice. We recorded GFP^+ neurons in motor area. (a-c) Miniature excitatory post-synaptic currents (mEPSC). (a) Representative traces, (b) frequency and (c) amplitude are shown. (d,e) Miniature excitatory post-synaptic currents (mIPSC), with representative traces (d), mean frequency (e) and amplitude (f). (g,h) Input resistance was increased (g) and capacitance decreased (h), indicating reduction of cell size. (i,j) Increased cell intrinsic excitability. (i) Example firing responses to +80 pA current steps in a WT (top) and a KO (down) cell. (j) NeuroD2 KO neurons reached action potential (AP) firing threshold earlier than matching WT neurons and exhibit a steeper input-output relationship, as assessed by the number of APs elicited by increasing current injections (from +40 to +100 pA, 20-pA increments) during current-clamp recordings. (k) After-hyperpolarization (AHP) was normal in NeuroD2 KO mice. (l,m) NeuroD2 KO neurons exhibit increased Ih-current amplitudes compared with matching WT neurons (current/voltage relation of Ih currents). Data are means ± SEM. Number of cells/ animals analyzed are shown in bars or parentheses. Statistical significance was evaluated by unpaired t-test for samples with normal distributions [bar graphs in (b), (c), and (f)], by Mann-Whitney test for non-normal samples [bar graph in (e)], and by two-way repeated measure ANOVA [(a), (b), (j) and (o)] followed by Bonferroni's post hoc test (*P <0.05; **P <0.01; ***P <0.001).

Figure 4: Behavioral phenotypes in NeuroD2 KO and heterozygous mice. (a-c) In the novel object recognition test (a), NeuroD2 KO and heterozygous mice displayed unaltered total investigation time (b) and discrimination index between the familiar and the novel object (c). (d-f) During social interaction in the three-chamber test (d), all genotypes displayed

unaltered total social investigation time (e). In contrast, while WT and heterozygous mice spent twice more time investigating the mouse than the empty quadrant, NeuroD2 KO mice spent equivalent times investigating mouse and empty quadrants (f). (g-i) Social memory/ interest test. When familiar and novel mice were placed in each quadrant, all genotypes spent similar times having social interactions (h), but only WT mice spent significantly more time investigating the novel mouse, indicating altered social memory in heterozygous and KO mice (i). (j) Rearing (left graph) and circling (right graph) behaviors in the 3 genotypes. (k) Hyperactivity in NeuroD2 KO mice. The graph depicts the distance traveled in 1 minute-intervals during 10 minutes in the open field. (l) Spontaneous seizures were observed in a third of NeuroD2 KO mice and in one heterozygous mouse during the course of the behavioral experiments, but never in WT littermates. (m, n) Time spent in the large center of the open field (red square in representative examples in m) was significantly increased in both heterozygous and KO mice (n). N= 16 WT, 15 heterozygous and 15 KO mice aged 8-14 weeks depending on the test. Data are means ± SEM. Statistical significance was evaluated by one-way ANOVA [(b), (c), (e), (h), (j) and (n)] or two-way ANOVA followed by Bonferroni's post hoc test [(f) and (i)] (n.s., not significant; *P<0.05; **P<0.01; ***P < 0.001).

Fig. 5: Characterization of NeuroD2 KO differentially expressed genes by RNA-seq. (a) Areas encompassing motor and somatosensory cortices were microdissected from coronal brain sections. (b) Number of differentially expressed genes associated with layer 2/3 (L2/3), L5 and L6, and overlaps between these groups. (c) ClueGO analysis of gene ontology indicates strongest enrichment in three biological processes: voltage-gated ion channel activity, chemical synaptic transmission and cell projection morphogenesis. (d,e) Fold change expressions (FC; log2 scale) of differentially expressed genes belonging to voltage-dependant ion channels (d) and synaptome (e) genes. In these histograms genes are ranked by expression change significance based on P-values (left: the most significantly differentially expressed). (f-h) Differentially expressed genes and neuropsychiatric disorders. (f) Heatmap showing synaptome and neuropsychiatric disorder-related genes differentially expressed in

NeuroD2 KO compared to WT mice. In red, genes with higher expression; in blue, genes with lower expression. (g) Overlaps between differentially expressed genes and gene sets of interest: synaptome, ASD, FMRP and ID. Number of genes for each gene sets are indicated. The table below shows overlap P-values for each gene set using binomial test. N=3 animals per genotype. (h) Fold change expressions (FC; log2 scale) of differentially expressed genes related to ASD, ordered by rank. Colors correspond to syndromes associated with selected genes.

Figure S1: Developmental expression of NeuroD2 mRNA and protein in the mouse cerebral cortex. (a-e) NeuroD2 mRNA is expressed throughout cortical development as revealed by in situ hybridization (Allen Brain Atlas). (f) qRT-PCR analysis of NeuroD2 expression during cerebral cortex development shows a peak of expression at E18.5 and a maintained expression postnatally. (g,h) NeuroD2 protein is expressed in the intermediate zone and cortical plate at E16.5 (g), and in layer 5 Ctip2^{+} PNs at P3 (h). (i) NeuroD2 protein never overlapped with Gad67-GFP, indicating absence of expression in inhibitory neurons. CP: cortical plate, IZ: intermediate zone, MZ: marginal zone, V/SVZ: ventricular/subventricolar zone. Sacle bars: g, ; h, ;i,.

Figure S2: Laminar distribution and axonal targeting identity of PNs-complement to Figure 1. (a-d) Laminar organization of somatosensory cortex at P28 was unaltered in NeuroD2 KO mice. (e,f) L1 immunostaining showed unaltered corpus callosum and other cortico-cortical axonal tracts in NeuroD2 KO mice. Sacle bars: e, ; f,.

Figure S3: Dendritic lengths in layer 5 PNs of NeuroD2 KO mice. (a,b) Total dendritic length (a) and dendritic length per level (b) in the basal compartment of WT (grey) and KO (red) mice. (c,d) Total dendritic length (c) and dendritic length per level (d) in the apical tuft compartment.

Figure S4: Spine subtypes in layer 5 PNs of NeuroD2 WT versus KO mice. (a,b) Density of spine subtypes in basal (a) and apical tuft (b) dendrites. (c) Neck diameter, head diameter and spine length were measured for thin, mushroom and stubby spines.

Figure S5: Resting potential and action potential properties of layer 5 PNs. (a) Resting membrane potential (Vrest), (b) action potential threshold and (c) action potential amplitude of NeuroD2 WT and KO neurons.

Figure S6: Behavioral phenotypes in NeuroD2 KO and heterozygous mice-complement to Figure 3. (a,b) Time in the mouse chamber (M), center chamber (C) and empty cage chamber (E) during the 10 minutes social interaction (a) and social memory (b) tests. (c) Distance traveled during 1 hour. (d,e) Resting time was decreased in both heterozygous and KO mice (d), but velocity (speed average when the animal is moving) was increased only in KO mice (e). (f,g) Detailed behavior during 10 minutes intervals over the 1 hour open field assessment, including resting (f) and distance (g).

Figure S7: Gene ontology with Cluego (Cytoscape). Pie charts representing main GO terms for all differentially-expressed genes (a), genes down-regulated in KO (b) and genes up-regulated in KO (c).

Figure S8: Fold changes of differentially expressed genes belonging to different cortical layers. Fold changes (FC; log2 scale) are shown for L6/subplate genes (a), L5 genes (b) and L2/3 genes (c). For each histogram genes were ranked for expression change significance based on P-values (left: the most significantly differentially expressed).

Figure S9: Differential expression of Syne1 isoforms in WT versus KO mice. The histogram shows amount of each Syne1 isoform in fragments per kilobase million (FPKM).

Data are means ± SEM. Statistical significance was evaluated by unpaired t-test with Welch correction (***P < 0.001).

Figure S10: Validation of RNA-seq data by qPCR and immunohistochemistry. (a) qPCR for ion channel and/ or neuropsychiatric genes. (b) Immunohistochemistry against Cplx3 protein on coronal brain sections at motor areal rostro-caudal level at 3 different ages (left), in WT versus KO conditions. Scale bar: .

Figure 1

NEUROD2 EXPRESSION IN PYRAMIDAL NEURONS

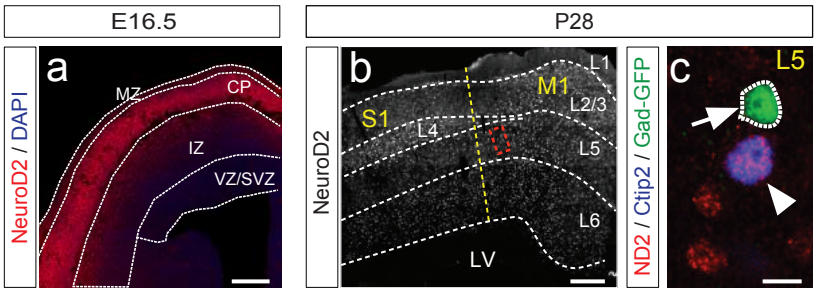

CORTICAL SIZE

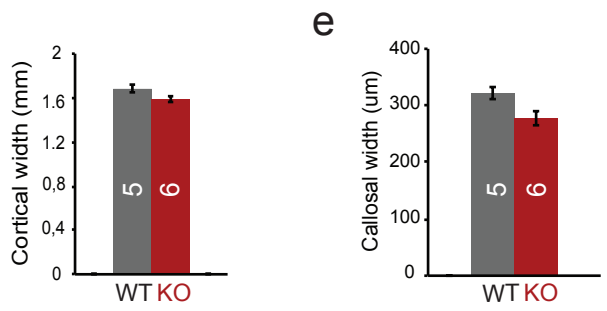

NEURONAL SUBTYPE DIFFERENTIATION AND LAMINATION

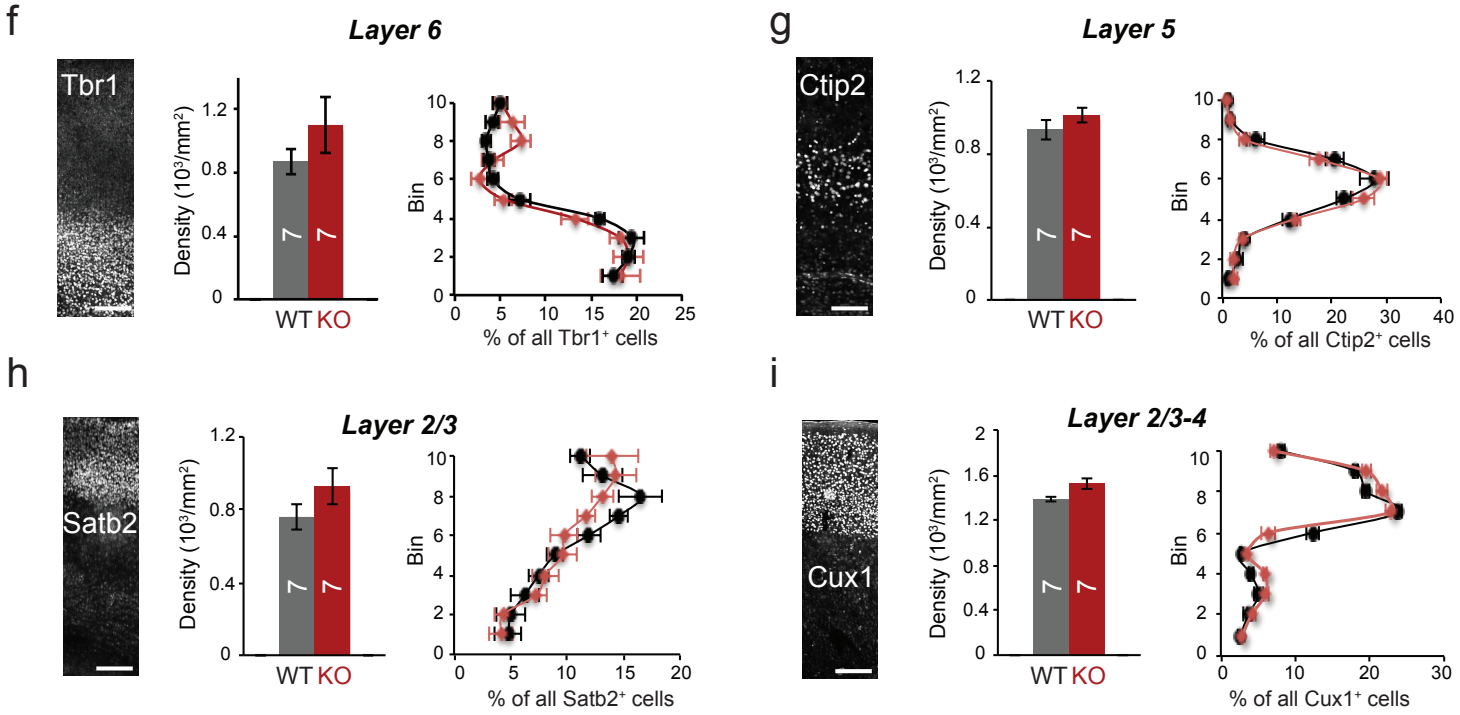

MIGRATION

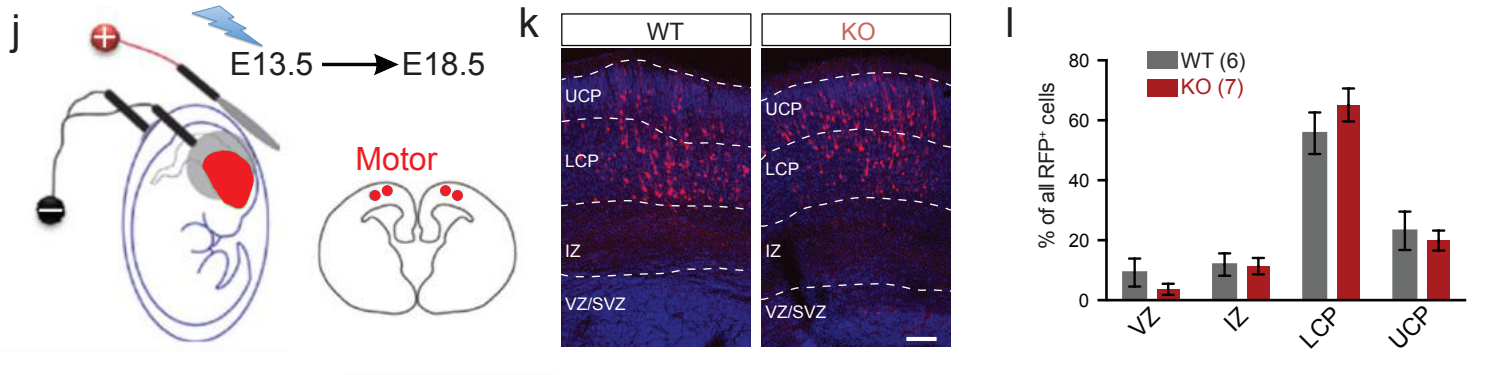

AXONAL TARGETING OF NEURONAL SUBTYPES

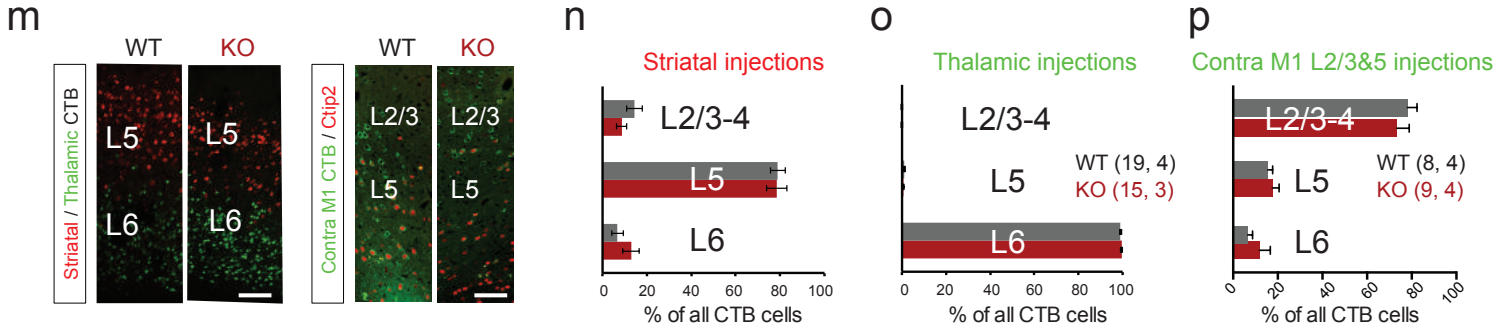

Figure 2

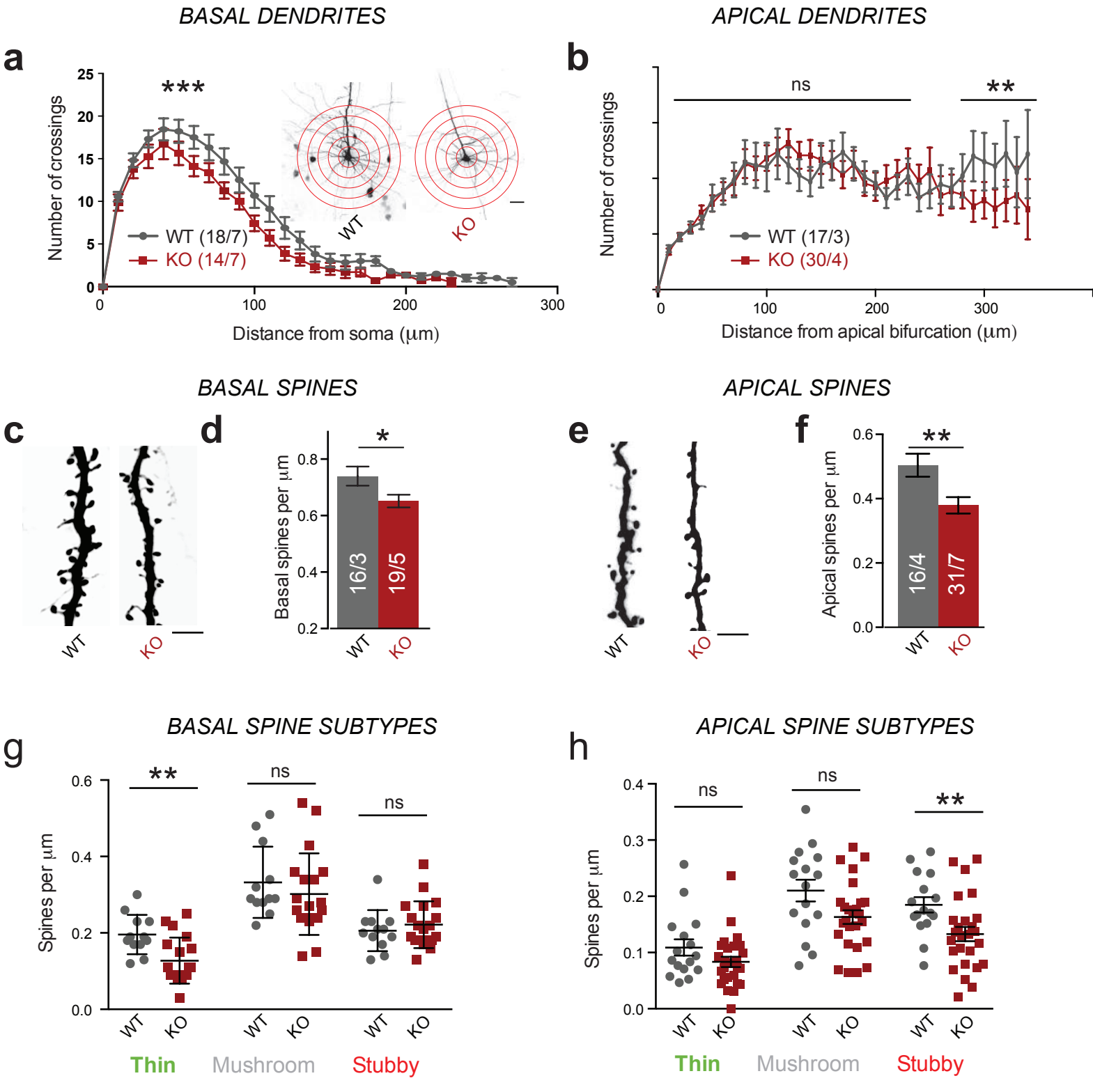

Figure 3

EXCITATORY INPUTS

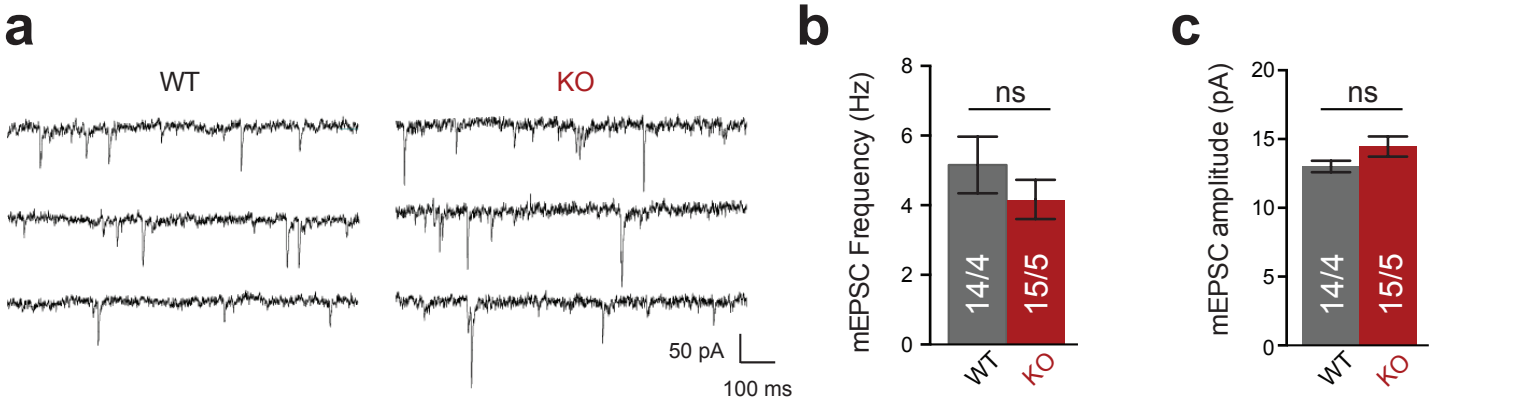

INHIBITORY INPUTS

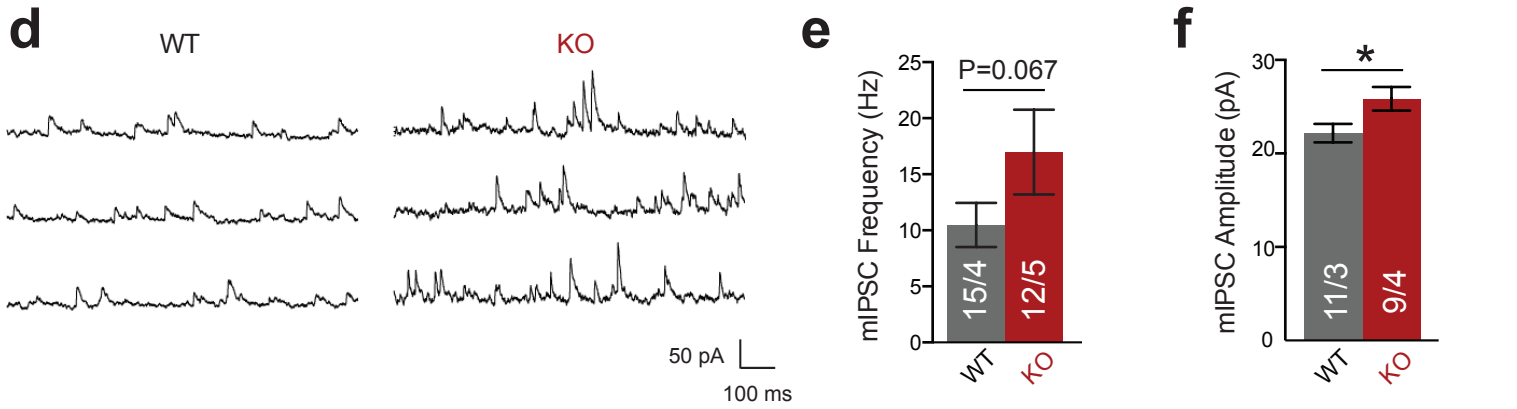

RESISTANCE & CAPACITANCE

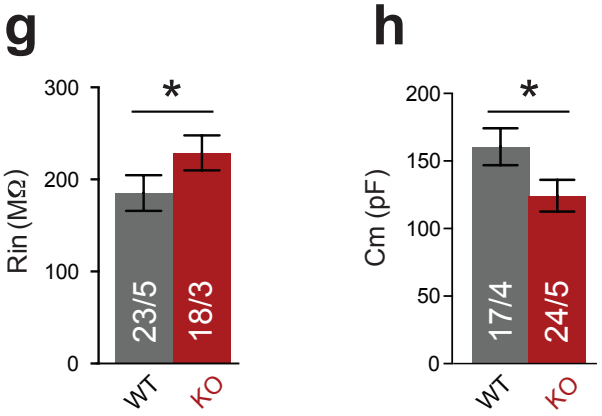

NEURONAL EXCITABILITY

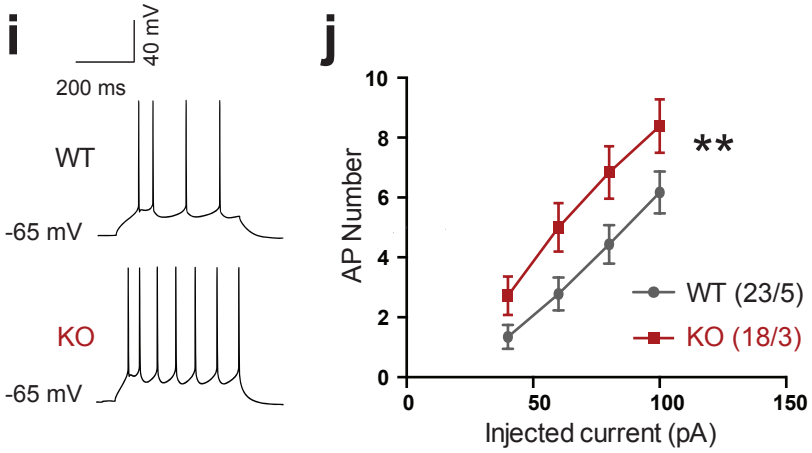

I_H CURRENT AMPLITUDE

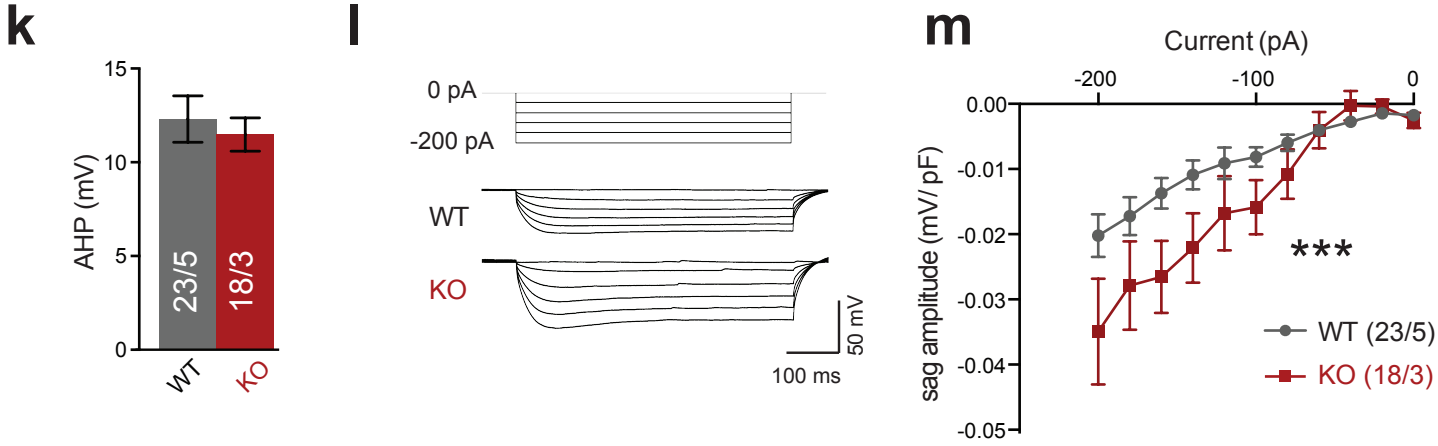

Figure 4

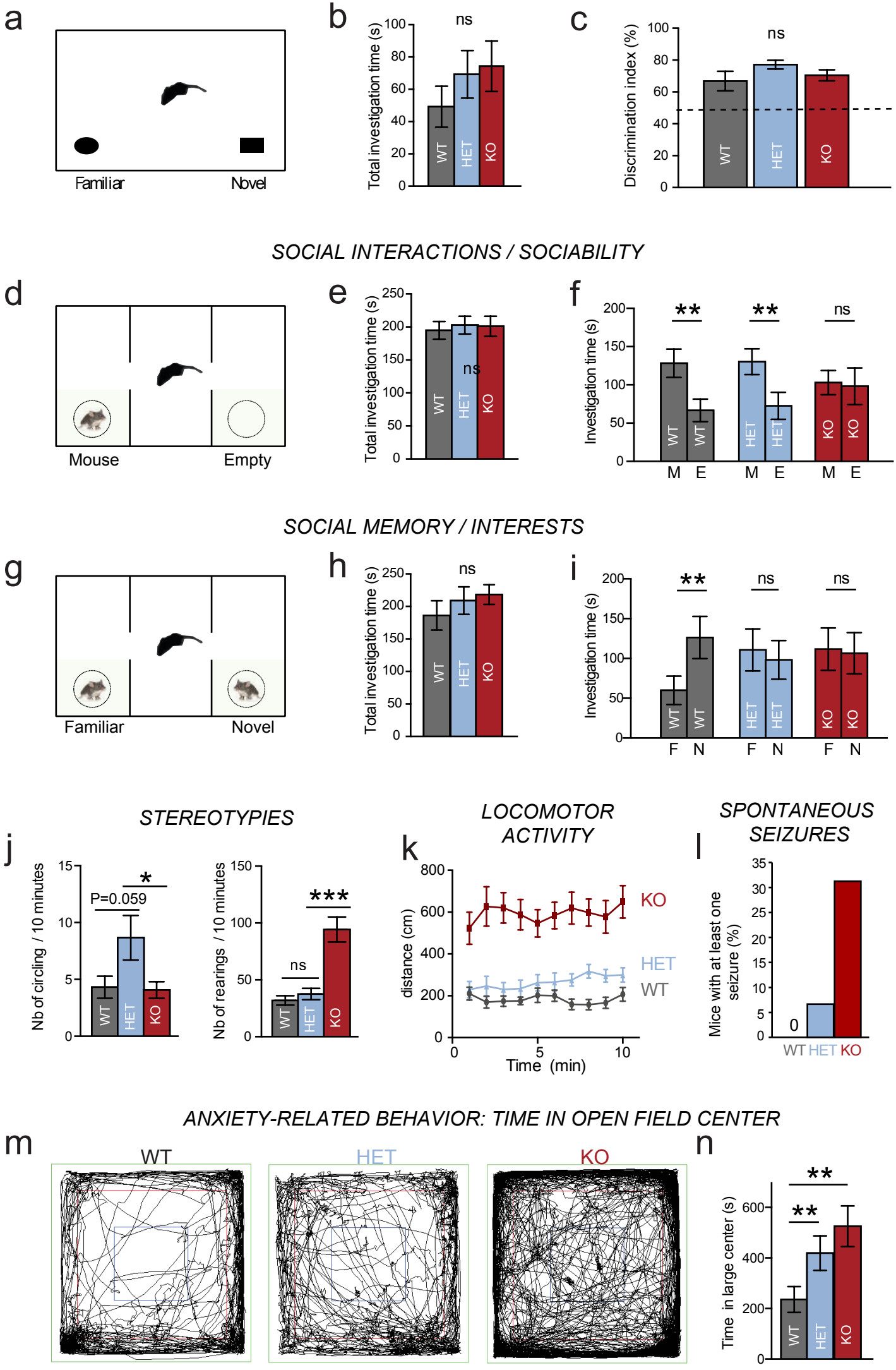

Figure 5

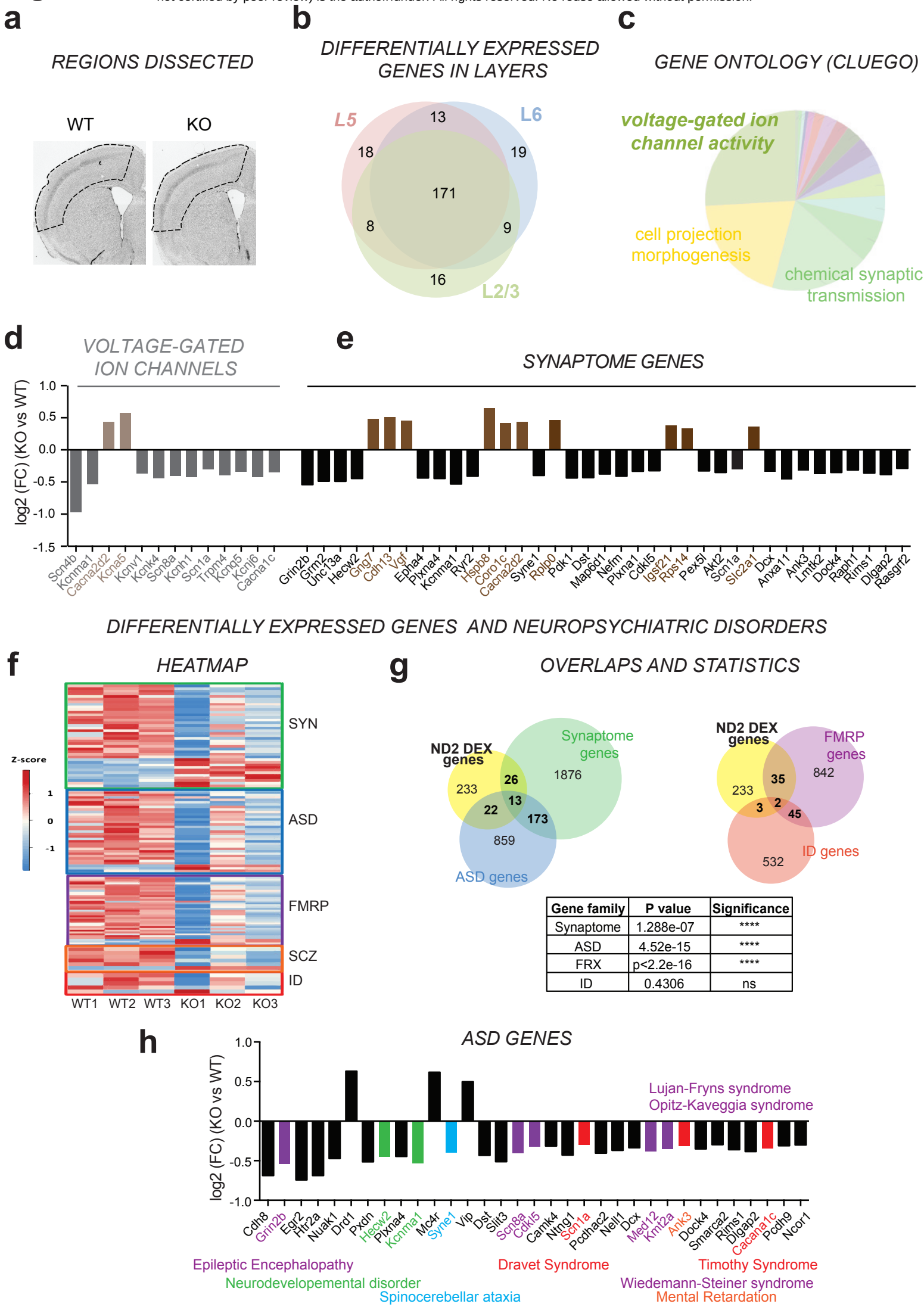

Gene family	P value	Significance
Synaptome	1.288e-07	****
ASD	4.52e-15	****
FRX	p<2.2e-16	****
ID	0.4306	ns

Figure S1

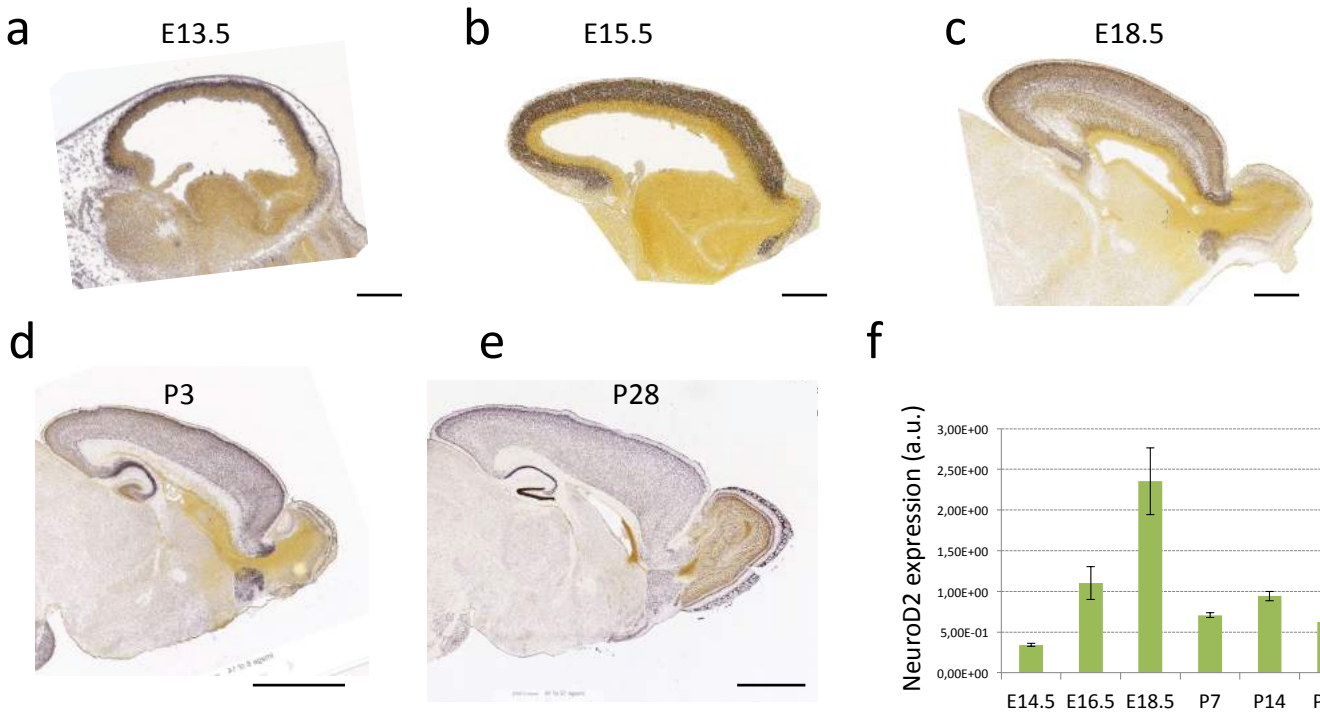

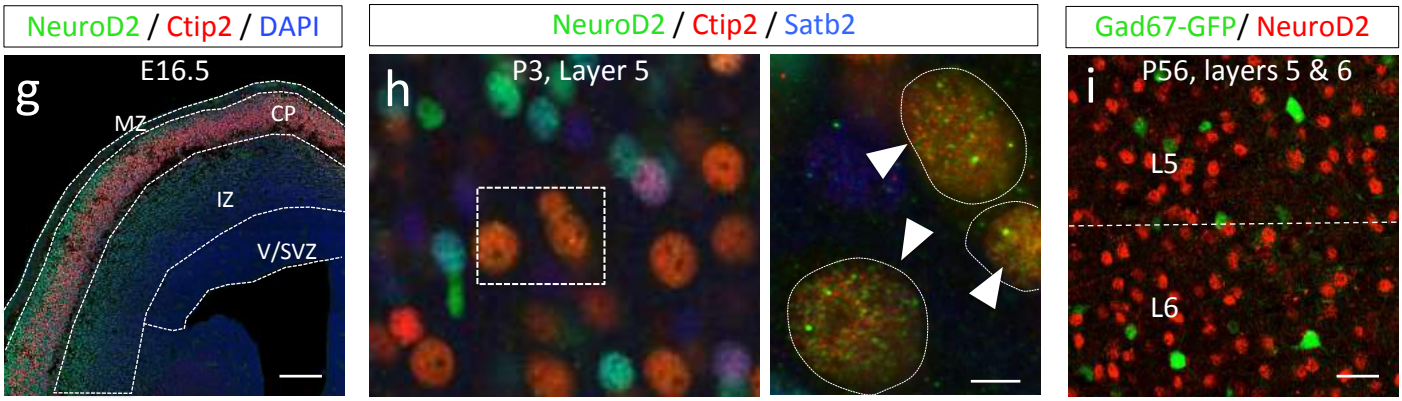

Figure S2

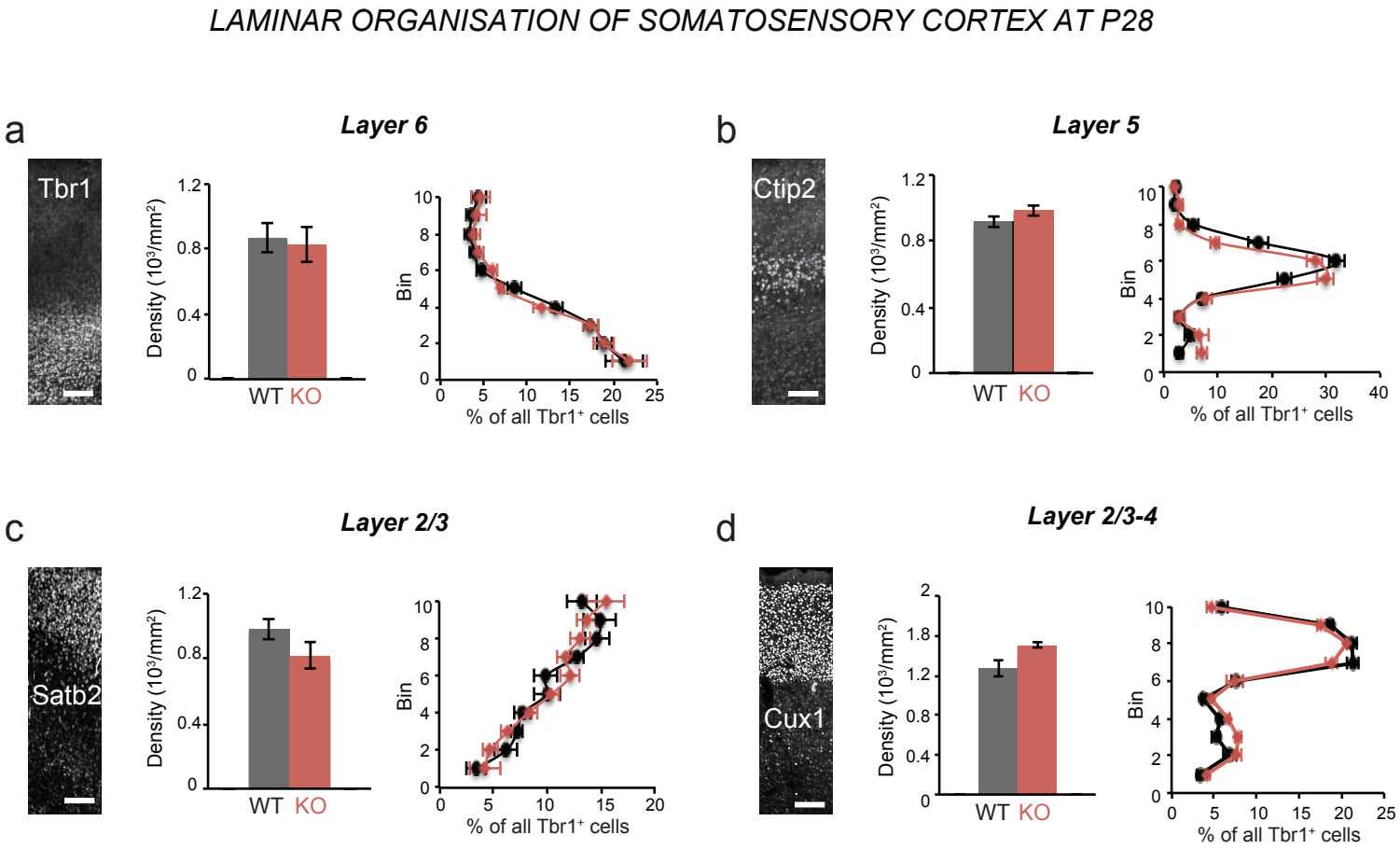

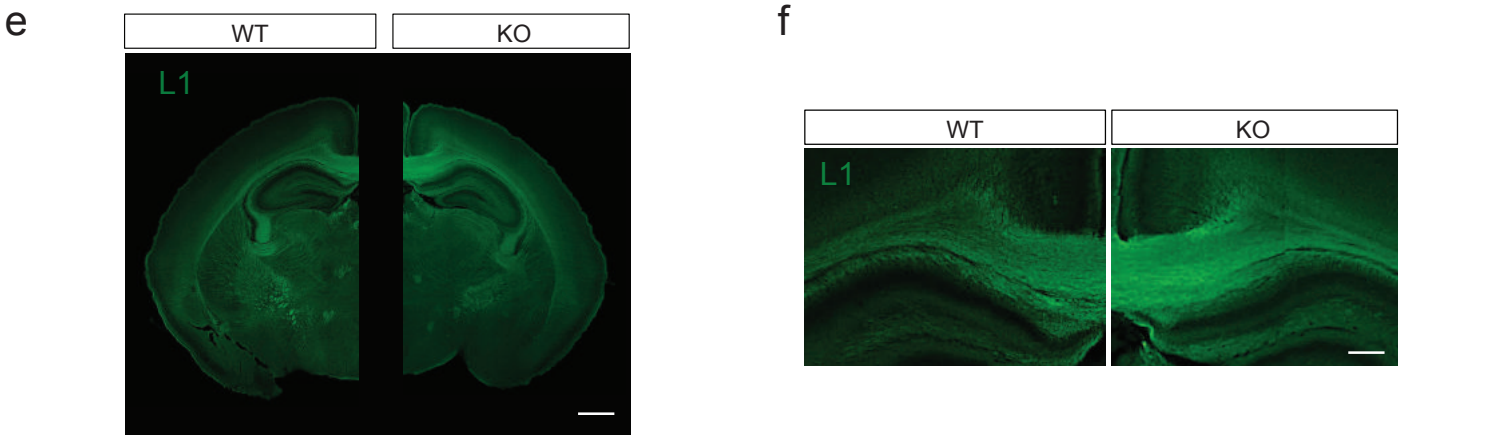

Figure S3

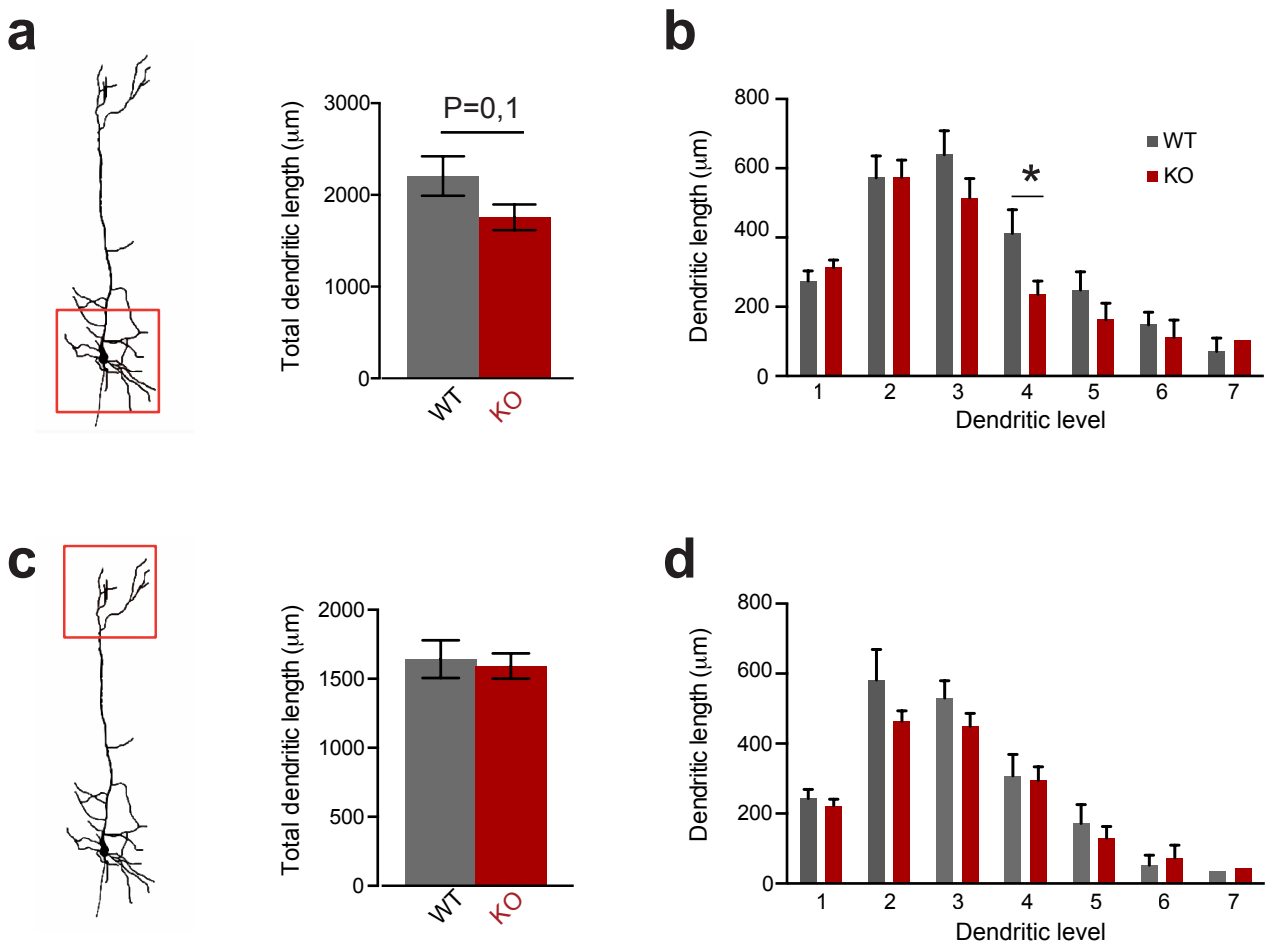

Figure S4

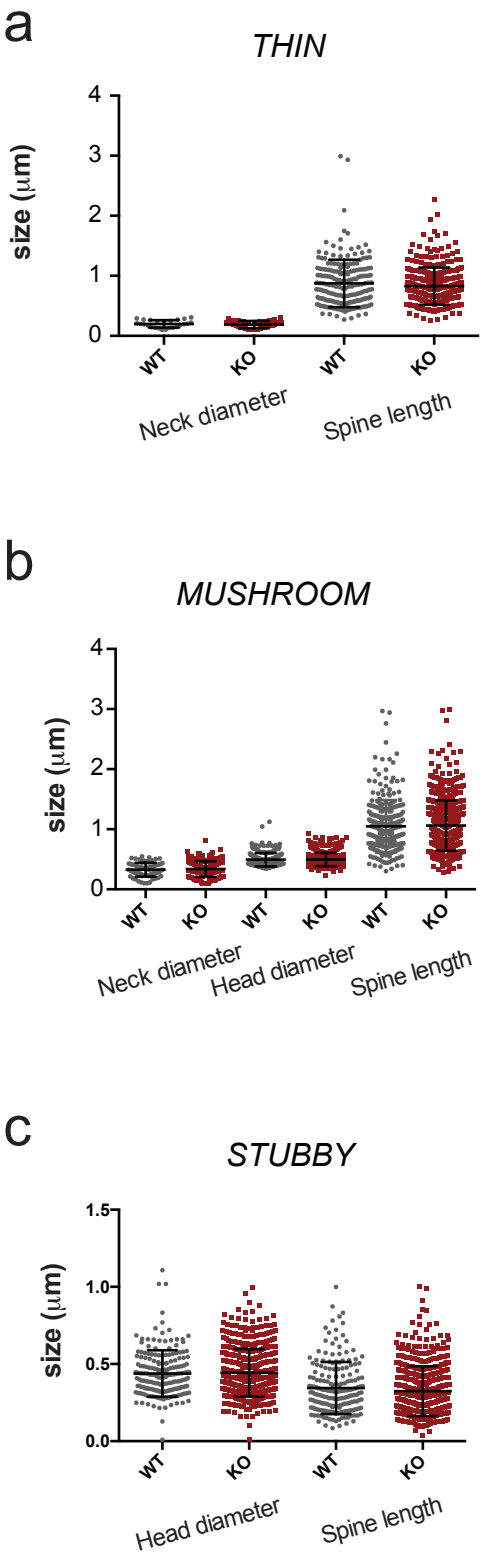

Figure S5

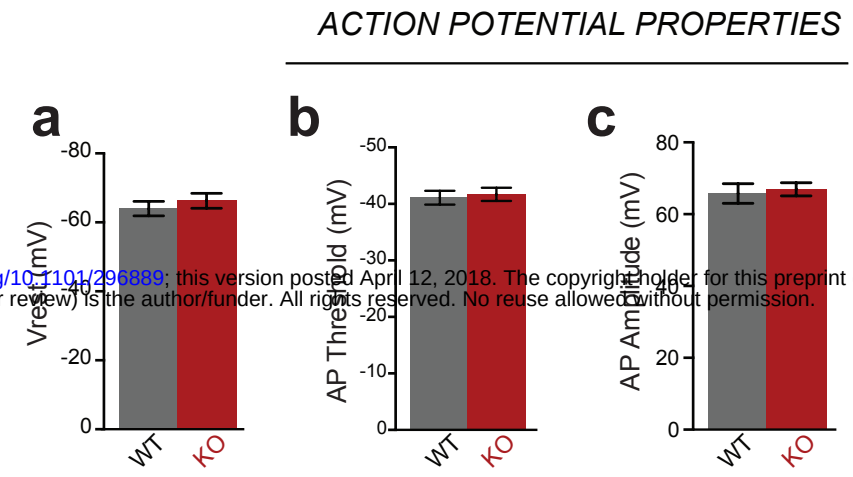

Figure S6

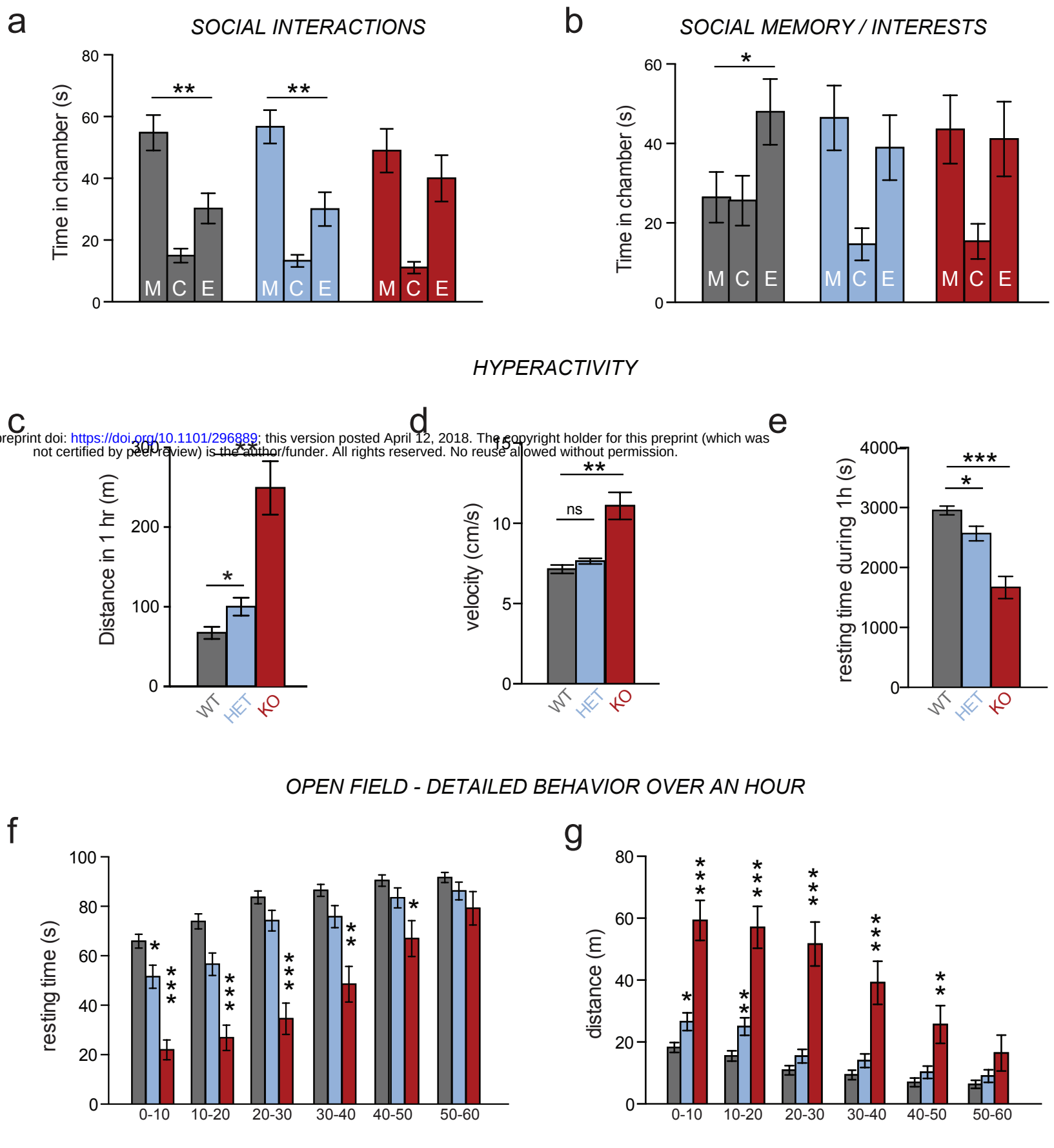

Figure S7

a

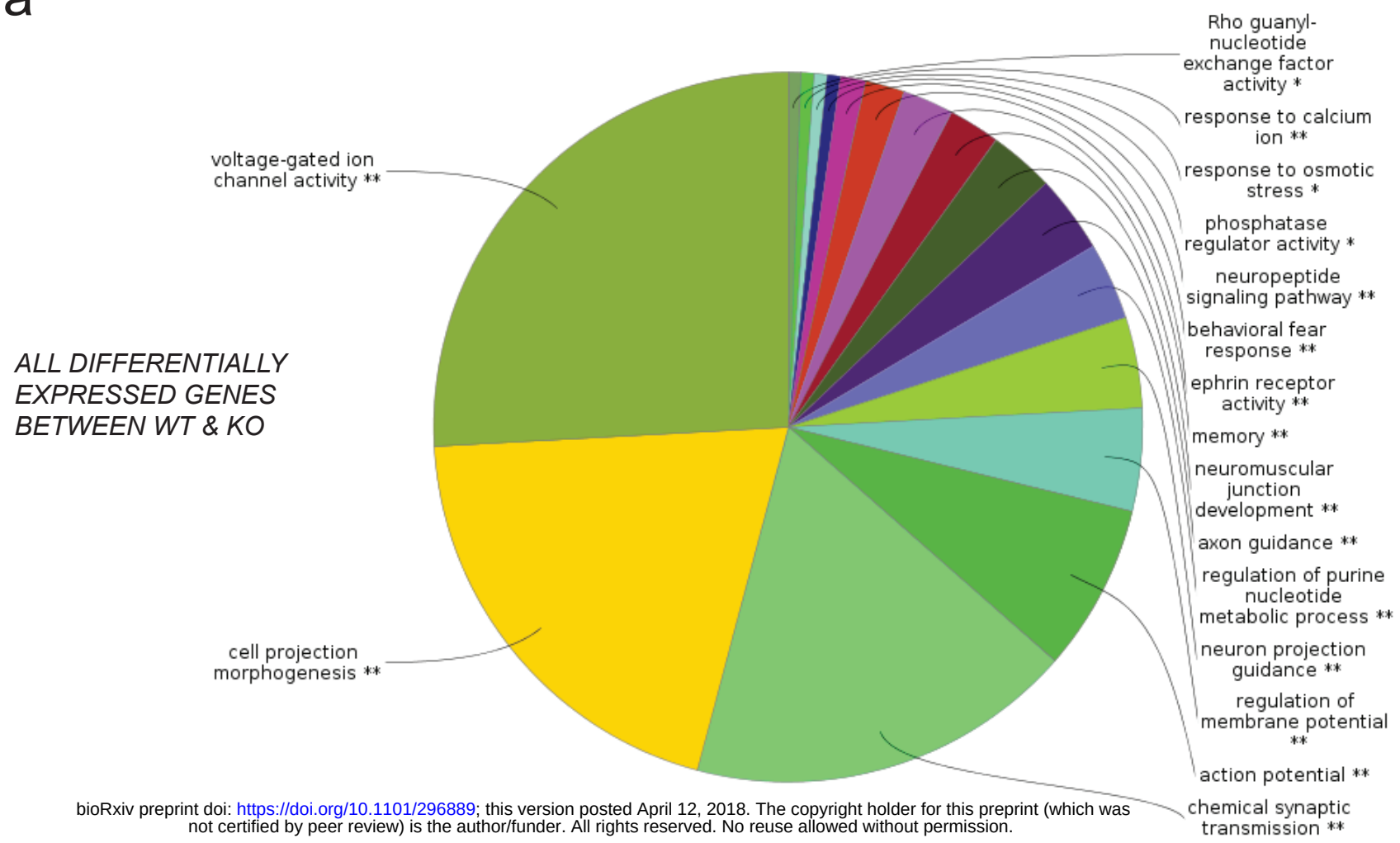

b

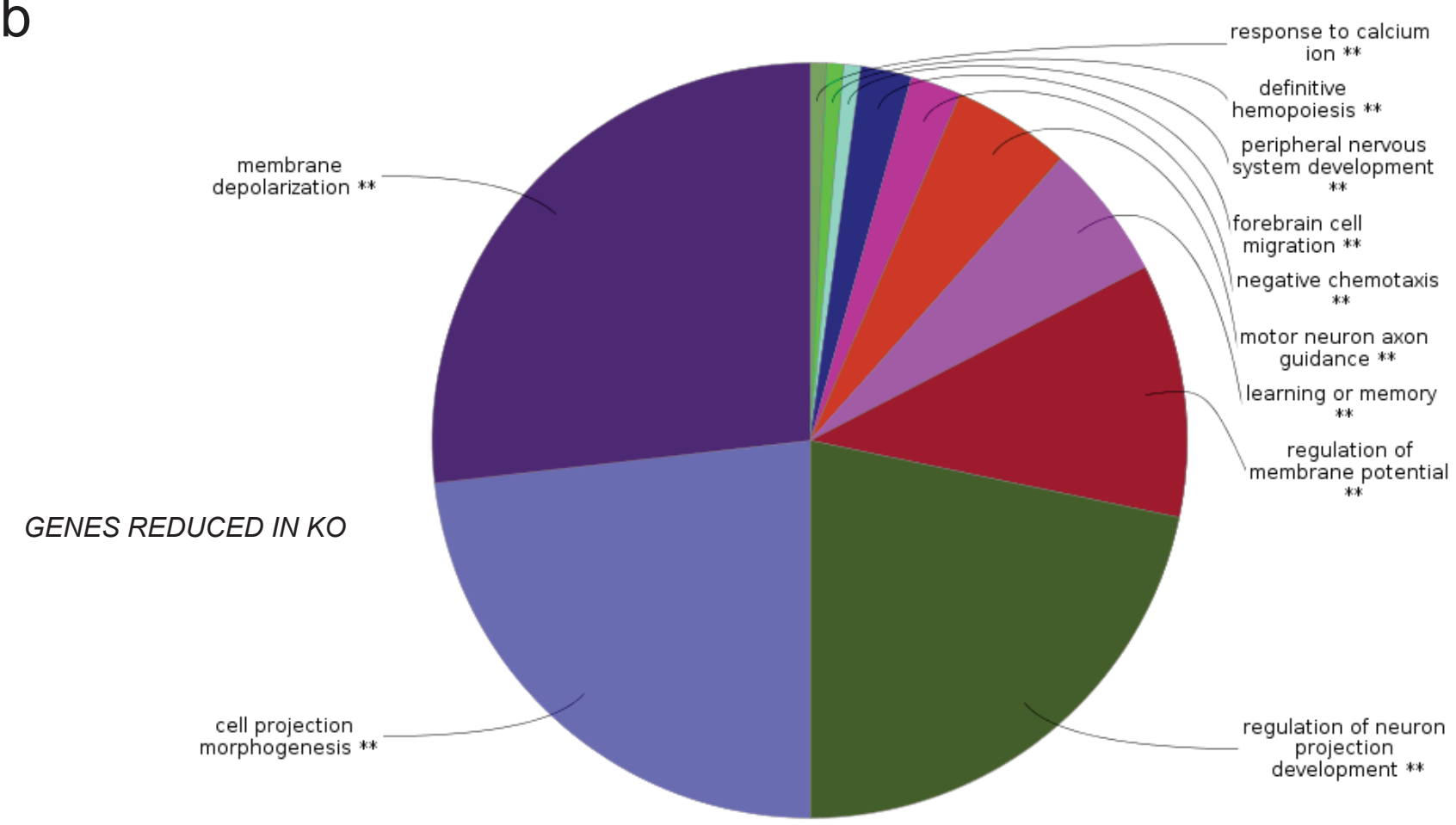

c

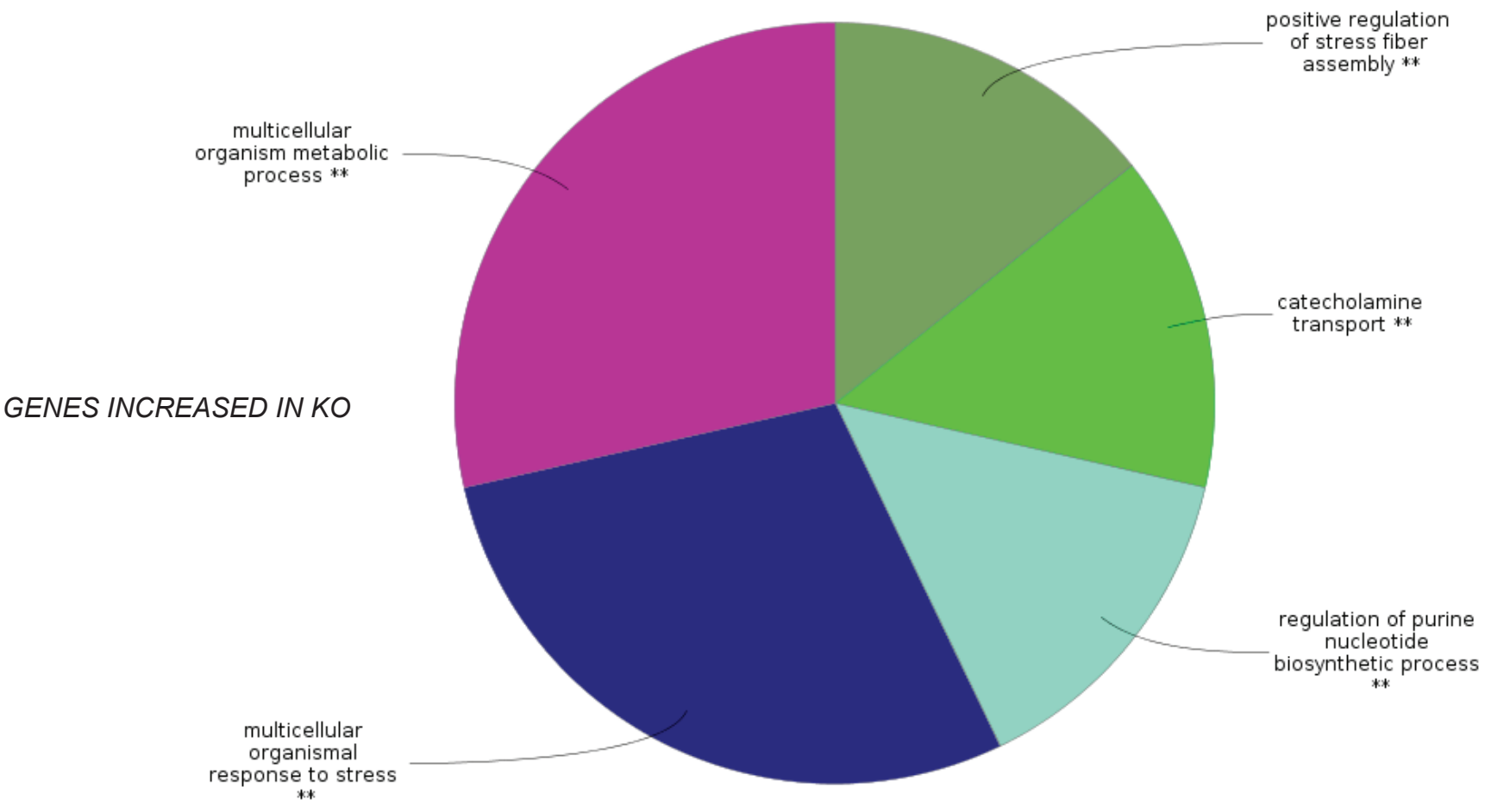

Figure S8

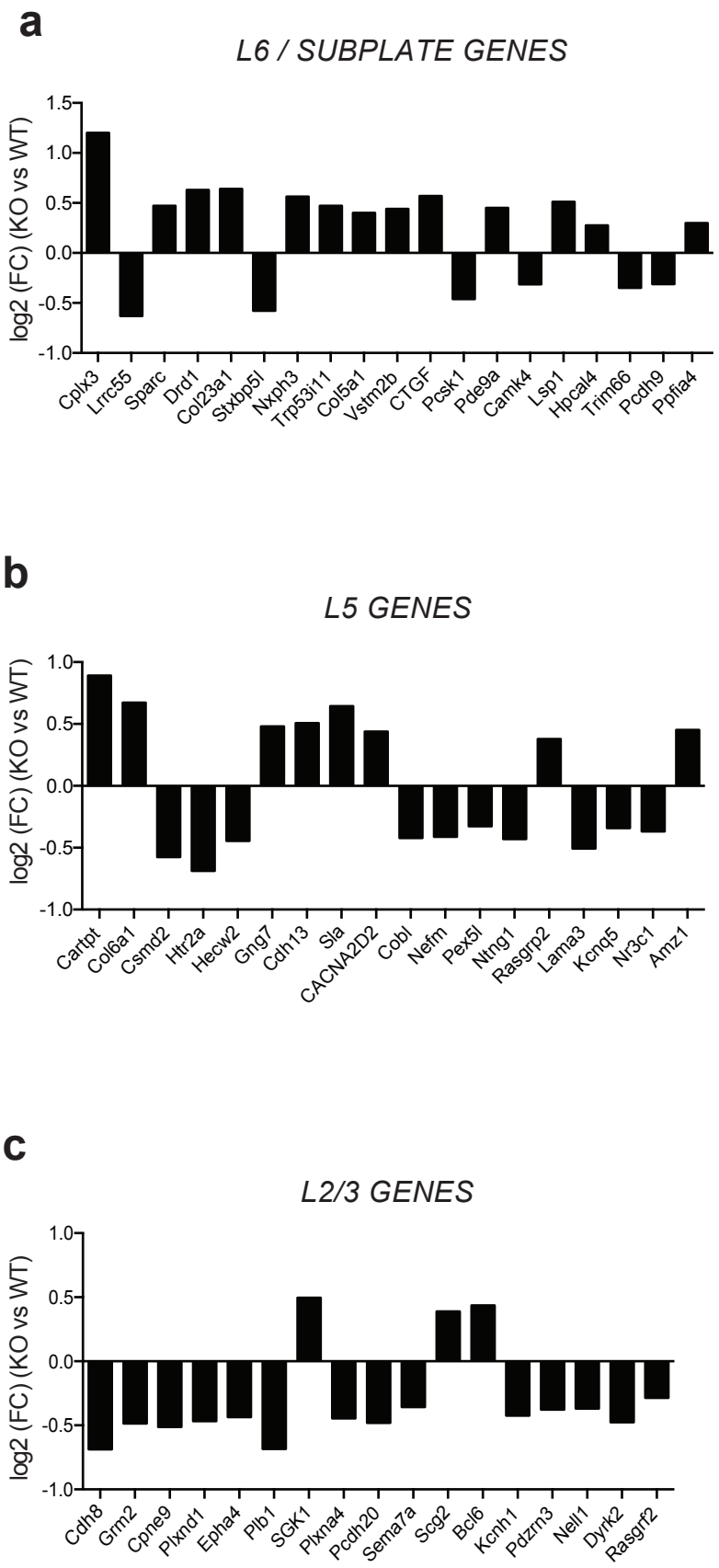

Figure S9

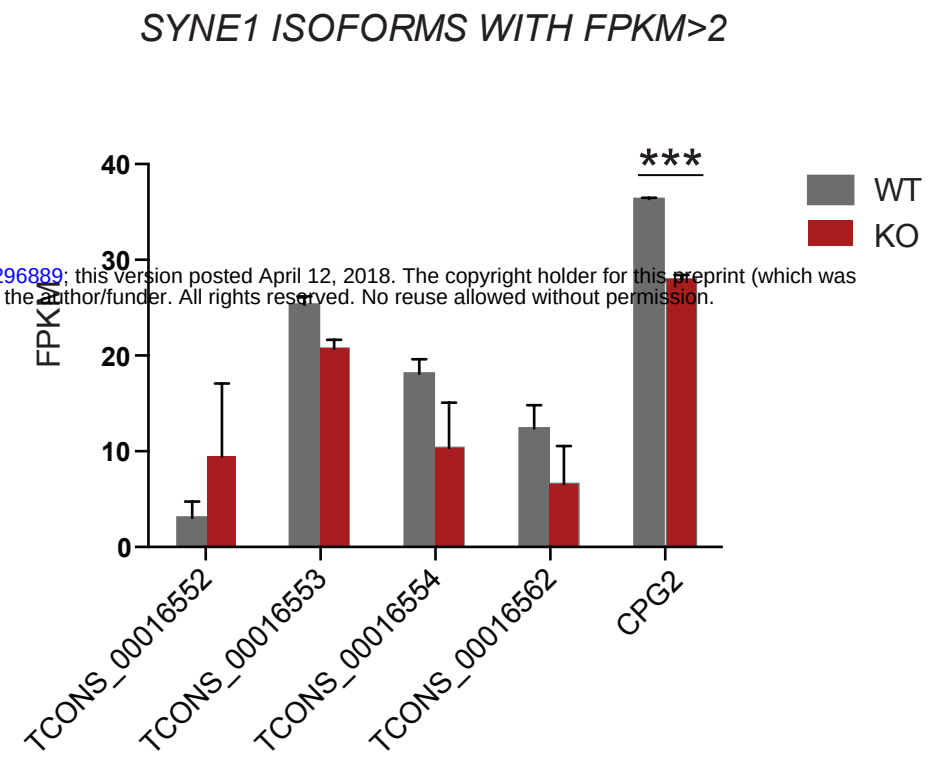

Figure S10

a

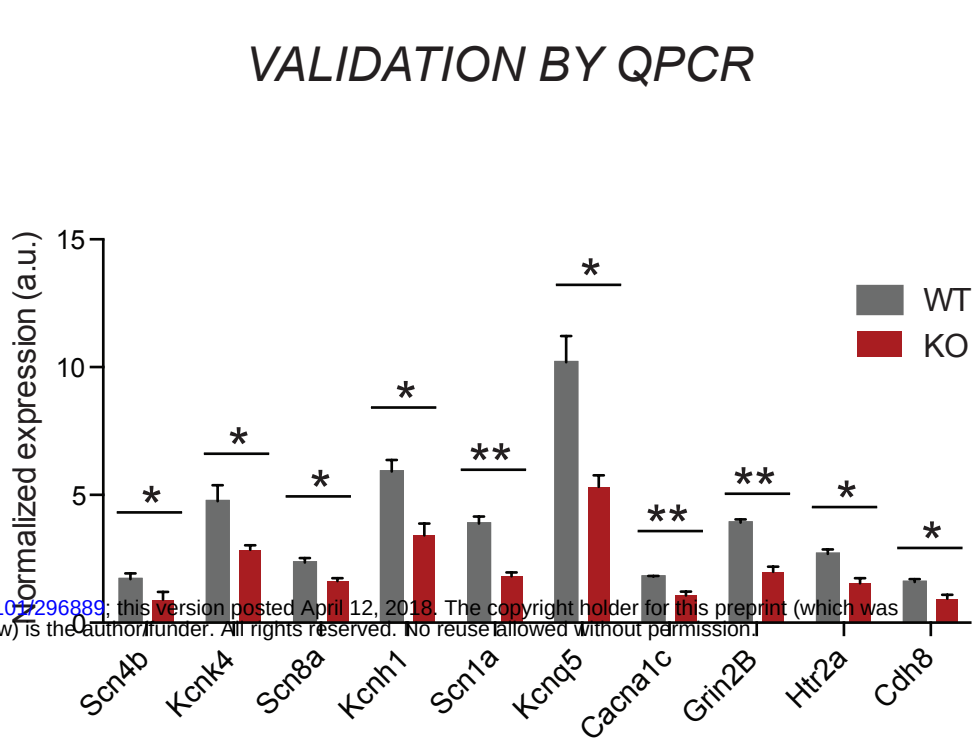

b